ARTICLES
https://doi.org/10.1038/s41593-018-0130-4
nature neuroscience

Cortical drive and thalamic feed-forward inhibition control thalamic output synchrony during absence seizures

Cian McCafferty[1,2,7*], François David[1,3,7], Marcello Venzi[1], Magor L. Lőrincz[4], Francis Delicata[1,5], Zoe Atherton[1], Gregorio Recchia[1], Gergely Orban[1,5], Régis C. Lambert[6], Giuseppe Di Giovanni[1,5], Nathalie Leresche[6] and Vincenzo Crunelli[1,5*]

Behaviorally and pathologically relevant cortico-thalamo-cortical oscillations are driven by diverse interacting cell-intrinsic and synaptic processes. However, the mechanism that gives rise to the paroxysmal oscillations of absence seizures (ASs) remains unknown. Here we report that, during ASs in behaving animals, cortico-thalamic excitation drives thalamic firing by preferentially eliciting tonic rather than T-type Ca^{2+} channel (T-channel)-dependent burst firing in thalamocortical (TC) neurons and by temporally framing thalamic output via feedforward reticular thalamic (NRT)-to-TC neuron inhibition. In TC neurons, overall ictal firing was markedly reduced and bursts rarely occurred. Moreover, blockade of T-channels in cortical and NRT neurons suppressed ASs, but such blockade in TC neurons had no effect on seizures or on ictal thalamic output synchrony. These results demonstrate ictal bidirectional cortico-thalamic communications and provide the first mechanistic understanding of cortico-thalamo-cortical network firing dynamics during ASs in behaving animals.

Cortico-thalamo-cortical circuits process behaviorally relevant internal and external information, determine vigilance states, and elicit diverse forms of neuronal network oscillations during sleep[1–3]. Reciprocal excitation between neocortex and thalamus allows the synchronization of these brain regions, while cortico-thalamic afferents also excite GABAergic nucleus reticularis thalami (NRT) neurons, thus driving feedforward inhibition of TC neurons[4]. Inhibition of TC neurons can evoke a rebound T-type Ca^{2+} channel (T-channel)-mediated burst of action potentials that in turn excites cortical targets, as well as exciting NRT neurons, leading to intrathalamic feedback inhibition[4]. This thalamic rhythmogenesis contributes to or determines many physiological cortico-thalamo-cortical oscillations[5]—in particular, those underlying spindle, slow-wave and delta oscillations of non-REM sleep that require T-channel bursts in both TC and NRT neurons[1,5,6].

The T-channel bursts of these thalamic neuronal populations are also considered essential for the thalamic rhythmogenesis of typical ASs, a type of non-convulsive seizure characterized by sudden loss of consciousness and spike-wave discharges (SWDs) in the electroencephalogram (EEG)[7–9]. Indeed, accepted AS mechanisms, supported by in vitro[10,11] and in silico[12,13] studies, require the presence of bursts in both TC and NRT neurons at each SWD cycle, with $GABA_A$ and/or $GABA_B$ receptors and intrinsic Ca^{2+}- and/or Na^+-activated K^+ currents contributing to the rhythmicity of these respective neuronal populations. However, these studies are limited by the compromised network integrity and absence of behavioral correlates inherent to in-vitro preparations. In contrast, studies that have examined the activity of thalamic neurons in intact animals under fentanyl or anesthesia report either a paucity of T-channel bursts in TC neurons[14] or the presence of two populations of TC neurons, one almost fully silent and the other with occasional bursts intermixed with single action potentials[15], whereas NRT neurons show bursts at each SWD cycle[15,16]. The relevance of these and other in vivo investigations using multi-unit activity[17] is also limited given the lack of behavioral seizures and the profound effects of fentanyl and anesthesia on SWD properties[18,19]. Thus, we still have no knowledge of the TC and NRT neuron firing dynamics and interactions during behavioral ASs.

Here, using ensemble recordings of single somatotopically aligned thalamic and cortical neurons during genetically determined or pharmacologically induced ASs in freely moving rats, we found complex temporal dynamics of TC and NRT neuron firing, with TC neurons exhibiting a marked decrease in overall firing and a paucity of burst firing. Selective blockade of T-channels in NRT and cortical neurons decreased ASs, whereas their block in TC neurons did not affect seizure expression. Cortical excitatory and NRT inhibitory input to TC neurons during seizures, as well as cortical excitation of NRT neurons, suggest a role for ictal feedforward inhibition of TC neurons. Taken together, these results demonstrate that during behavioral ASs the synchronous, seizure-perpetuating output of TC neurons is not determined by the dynamics of their T-channel-mediated burst firing but rather is driven by top-down cortical excitation and sharpened by cortically driven, T-channel-dependent NRT inhibition.

Results

Ensemble recordings of single thalamic neurons during ASs. Using microdrive-mounted silicon probes (Supplementary Fig. 1d),

[1]Neuroscience Division, School of Bioscience, Cardiff University, Cardiff, UK. [2]Department of Neurology, Yale University School of Medicine, New Haven, CT, USA. [3]Team Waking, Lyon Neuroscience Research Center, CRNL, INSERM U1028, CNRS UMR5292, University of Lyon 1, Lyon, France. [4]Department of Physiology, Anatomy and Neuroscience, University of Szeged, Szeged, Hungary. [5]Department of Physiology and Biochemistry, University of Malta, Msida, Malta. [6]Sorbonne Université, CNRS, Inserm, Neuroscience Paris Seine – Institut de Biologie Paris Seine (NPS – IBPS), Paris, France. [7]These authors contributed equally: Cian McCafferty, François David. *e-mail: mccaffertycp@cardiff.ac.uk; crunelli@cardiff.ac.uk

alone or with microdialysis probe(s)[20], we studied under freely moving conditions the interictal (between seizures) and ictal (during seizures) firing dynamics of TC neurons of the ventrobasal thalamic nucleus (VB) and NRT neurons in two well-established AS models: the Genetic Absence Epilepsy Rats from Strasbourg (GAERS)[19] and the pharmacological γ-hydroxybutyrate (GHB) model[21] (Methods). The VB was chosen because the somatosensory system has a crucial role in ASs of these models, wherein SWDs originate from a cortical initiation site, the perioral region of primary somatosensory cortex (S1pO)[22,23], before spreading to the VB and then to other cortical regions (Supplementary Fig. 2). Individual action potential waveforms were isolated from the full-band raw signal, semiautomatically clustered following systematic visual inspection[24] (Fig. 1 and Supplementary Fig. 1a) and classified as originating from excitatory (i.e., TC) or inhibitory (i.e., NRT) neurons based on standard criteria[25] (Fig. 1b–d). Reliable identification of thalamic T-channel bursts during ASs was demonstrated by (i) the agreement of burst signatures (Fig. 1c) and action potential waveforms (Fig. 1d) with those currently used in TC and NRT neuron classification[25] and (ii) the similarity of burst features of each isolated neuron during periods of varying synchrony—i.e., seizures and sleep (compare Fig. 1c and Supplementary Fig. 1e; see Supplementary Fig. 3d and Methods).

TC neuron ictal activity. We recorded 139 TC neurons in 6 GAERS rats during 4,214 ASs (duration: 11.5 ± 4.4 s, mean ± s.e.m.) with a SWD frequency of 7.1 ± 0.5 Hz. Single TC neurons were markedly less active (52%) ictally than interictally (5.44 ± 0.03 vs. 11.4 ± 0.04 Hz, $P < 0.001$) (Fig. 2a–c and Supplementary Table 1), an effect driven by a reduction in tonic firing (2.8 ± 0.01 vs. 9.3 ± 0.03 Hz, $P < 0.001$) (Fig. 2e) and a large incidence of electrical silence: 45% of TC neurons (62 of 139) were silent for >50% of spike-and-wave complexes (SWCs), the individual cycles of SWDs (Fig. 3a). The decrease of total and tonic firing started 2 s before SWD detection in the EEG (Fig. 2c,e). By contrast, the interictal rate (0.40 ± 0.01 Hz) of T-channel bursts started to increase rapidly 1 s before seizure onset, peaked (1.8 ± 0.22 Hz) just after seizure onset (400 ms) and then decayed within the next 2 s to a stable level (0.9 ± 0.01 Hz, $P < 0.05$ compared to interictal) for the remainder of a seizure (Fig. 2d,f–h). Thus, the ictal incidence of bursts was low (15.7 ± 0.1% of SWCs) (Fig. 3b,e) while tonic firing occurred during 30.1 ± 0.1% of SWCs (Fig. 3c,f), leading to a total firing rate of 0.85 ± 0.01 spikes/SWC (Fig. 3d). Notably, despite the scarce ictal firing of individual TC neurons, there was a strong and rhythmic ictal thalamic output as indicated by the cross-correlograms (XCors) of simultaneously recorded TC neurons (Supplementary Fig. 4a). Moreover, the absolute and relative rates of tonic and burst firing of individual TC neurons could greatly vary between seizures (Supplementary Fig. 5). In summary, the firing of single TC neurons during ASs in behaving GAERS rats is characterized by (i) multistaged temporal dynamics, (ii) a marked decrease in total and tonic firing, and (iii) an increase in burst rate, though bursts occur only at every seventh SWC.

NRT neuron ictal activity. Two classes of NRT neurons could be identified on the basis of their firing during awake interictal periods[26]: wake-active (WA, >10 Hz) and wake-quiescent (WQ, ≤10 Hz) (Supplementary Fig. 1b). The total firing (47 ± 1.8 Hz) of WA NRT neurons ($n = 13$) in GAERS rats started to decrease 3 s before SWD detection, reached a minimum of 31 ± 0.9 Hz (500 ms before SWD detection) ($P < 0.01$) and then, in contrast to that of TC neurons, sharply increased to a peak of 62.1 ± 0.2 Hz ($P < 0.01$) at the interictal-to-ictal transition (Fig. 2c,i,j and Supplementary Table 1). Then it slowly decreased to a stable ictal level of 52 ± 2 Hz ($P = 0.032$ compared to interictal) (Fig. 2c). In contrast, tonic firing (25 ± 1 Hz) started to decrease 3 s before SWD detection, reaching a stable value of 14 ± 2 Hz ($P < 0.001$) (Fig. 2e). This decrease in WA NRT neuron tonic firing was overcompensated for by an enhancement of burst firing, which started to increase (from 0.31 ± 0.01 Hz interictally) at the same time as TC neuron bursts, peaked (2.4 ± 0.02 Hz, $P = 0.002$) about 2.5 s after seizure onset and then slowly decreased for the remainder of a seizure (1.4 ± 0.03 Hz at the ictal-to-interictal transition) (Fig. 2d,i,j). Although bursts in WA NRT neurons occurred on average during 25 ± 2% of SWCs, a group of neurons showed bursts in about 50% of SWCs and another group in <1% (Fig. 3g). Tonic firing was present during 53 ± 2.5% of SWCs, and the ictal total firing of WA NRT neurons was 6.2 ± 0.3 spikes/SWC (Fig. 3g,h).

Since WQ NRT neurons ($n = 12$) did not show any significant AS-associated variation in firing (Fig. 2), or any significant AS-linked feature in subsequent analyses (Supplementary Fig. 6), they will not be discussed hereafter, and WA NRT neurons will be referred to as NRT neurons. In summary, the firing of GAERS NRT neurons during ASs exhibited (i) multi-staged temporal dynamics and (ii) increased total and burst firing rates. However, in individual NRT neurons bursts did not occur at every SWC.

Synchrony and coherence of ictal thalamic neuron firing. Having characterized the firing dynamics of individual thalamic neurons during ASs, we investigated the synchrony and communication strength between TC and NRT neuronal ensembles. SWC-spike-triggered averages indicated that GAERS TC and NRT neuron total firing peaked 15 ms before and 9 ms after the SWC spike, respectively (Fig. 4a and Supplementary Table 2), although the initial ascending phase of the two population curves showed a strong overlap. Burst and tonic firing peaks had similar shape and latency (to the SWC-spike) to those of total firing (Fig. 4a).

However, SWC-spike-triggered averages are affected by the coherence and the amount of neuronal firing, an issue of critical importance here in view of the marked firing differences between the two thalamic populations. Notably, cumulative distribution functions of peak firing times relative to the SWC spike, which are unaffected by these properties, were similar for TC and NRT neurons (Fig. 4b) ($P = 0.631$; Kolmogorov–Smirnov test). This suggests that the TC and NRT populations are excited by a common source.

To understand interactions between the firing mode and the EEG paroxysmal oscillation, we analyzed the coherence of TC and NRT neuron firing with the SWC spike. TC neurons whose total firing peak was just before the SWC spike (–20 to 0 ms) were highly coherent compared to those whose peak was outside this window (Fig. 4c). In contrast, NRT neurons with a firing peak before the SWC spike showed very low coherence whereas those that preferentially fired after the SWC spike had high coherence (Fig. 4c). Moreover, TC neuron coherence was little influenced by firing type (Fig. 4e), whereas NRT neurons showed significantly higher coherence ($P < 0.001$) when they fired bursts (Fig. 4f). Consistently, NRT neurons with more overall burst firing were more coherent with respect to the SWC spike (Fig. 4d) whereas for TC neurons a high burst rate was not necessary for high coherence (data not shown).

In summary, GAERS TC and NRT neurons show synchronous activation with respect to the SWC spike. Furthermore, whereas NRT burst firing is more coherent than tonic, TC neurons have similar coherence for both firing types, suggesting that TC neuron bursts are not essential for paroxysmal synchrony.

Recruitment of intrathalamic inhibition. The paucity of TC neuron bursts, the high coherence of their tonic firing with SWDs, and the overlap of TC and NRT cumulative firing probabilities challenge the view that TC neuron bursts are necessary to drive cortical and NRT populations during seizure[10,11,13]. Thus, it was important to investigate the synaptic interactions between the two thalamic neuronal populations during ASs. XCors of the ictal firing of simultaneously recorded TC and NRT neuron pairs ($n = 14$) had broad

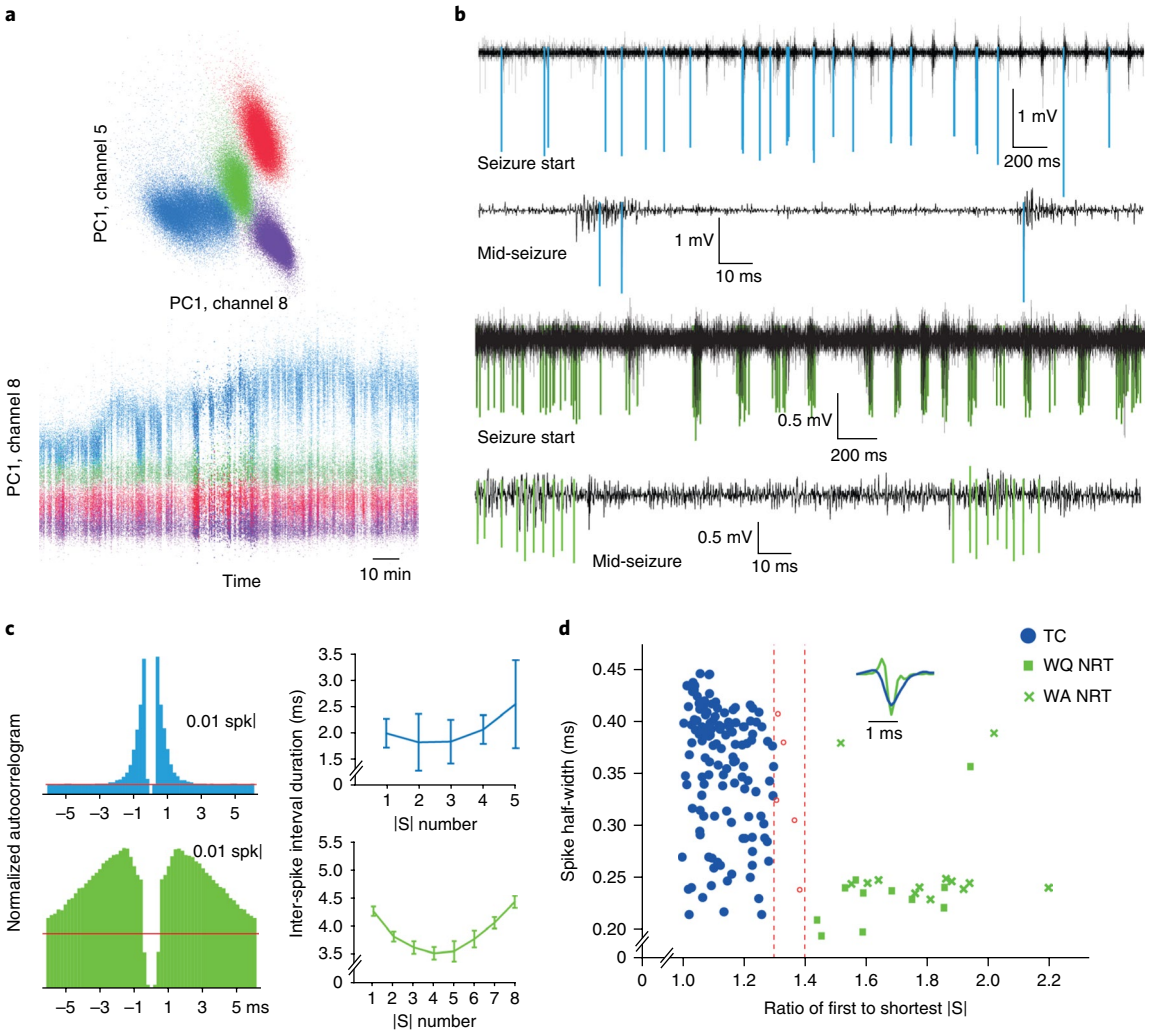

Fig. 1 | Spike clustering and thalamic neuronal type identification. a, Automated spike sorting by clustering of principal components (PC) in multiple dimensions, reflecting spike amplitude and spike shape. **b**, High-pass filtered traces showing typical isolated action potentials of TC (blue, top two traces) and NRT (green, bottom two traces) neuron spikes at start and middle of ASs. **c**, Autocorrelograms (left) and plots of mean interspike interval (ISI) versus interspike number of high frequency bursts (right) for a TC (blue) and an NRT (green) neuron during ASs. Error bars indicate ± s.e.m. Note the clear NRT neuron accelerando–decelerando pattern. **d**, Spike half-width vs. burst acceleration index (ratio of first to shortest ISI in a burst) for all neurons. Red dashed lines indicate acceleration index <1.3 for TC ($n = 139$) and >1.4 for NRT ($n = 25$) neurons used to identify the two neuron types (Methods). Neurons marked in red were excluded from further analysis. Inset depicts superimposed typical TC (blue) and NRT (green) spike waveforms.

peaks, often before time zero (Fig. 5a and Supplementary Fig. 6a), indicating an increased probability of NRT neurons firing after TC neurons. Those peaks were absent during interictal periods (Fig. 5f) and reduced during non-REM sleep (Fig. 5g).

Thirty-six percent (5 of 14) of GAERS TC–NRT pairs showed a significant post-zero trough indicating a decreased TC neuron firing probability following an NRT action potential (Fig. 5a), and thus an ictally active NRT–TC inhibitory connection. These inhibitory patterns were still present in XCors between TC neuron total firing and NRT neuron bursts (Fig. 5b), but were absent in XCors calculated using NRT neuron tonic firing (Fig. 5d), demonstrating that the decreased firing probability of TC neurons depends on NRT neuron bursts[10]. In contrast, the troughs were still present when TC neuron tonic firing was used for the XCors, indicating that TC neuron bursts are not required for these ictal intrathalamic interactions (Fig. 5c). Notably, NRT neurons that had relatively flat autocorrelograms showed neither significant peaks nor troughs in their XCors with TC neurons (Supplementary Fig. 6a–e). In summary, ASs involve intrathalamic inhibition via the recruitment of NRT–TC neuron inhibitory assemblies, which are dependent on NRT but not TC neuron burst firing. TC and NRT neurons of the GHB model had similar ictal firing dynamics, distributions and XCors those of the GAERS model (Supplementary Figs. 7 and 8 and Supplementary Tables 1 and 2).

Cortico-thalamo-cortical drive and feedforward inhibition. The lack of evidence for a TC neuron burst-dependent excitatory drive of NRT neurons (Fig. 5e), together with the similar ictal firing distributions of TC and NRT neurons (Fig. 4b), suggests that the corticofugal input may be a key source of excitation of both thalamic neuron populations, thus leading to intrathalamic feedforward inhibition. To directly investigate this possibility, we next simultaneously recorded thalamic and somatotopically aligned (Methods) putative pyramidal neurons in the S1pO cortical region of three GAERS rats (see Supplementary Fig. 9 for cortical neuron isolation and classification). Multiple pairs (13 of 58) of TC and cortical excitatory neurons showed two peaks in their ictal total firing XCors, suggesting bidirectional excitation (Fig. 6a). XCors that included

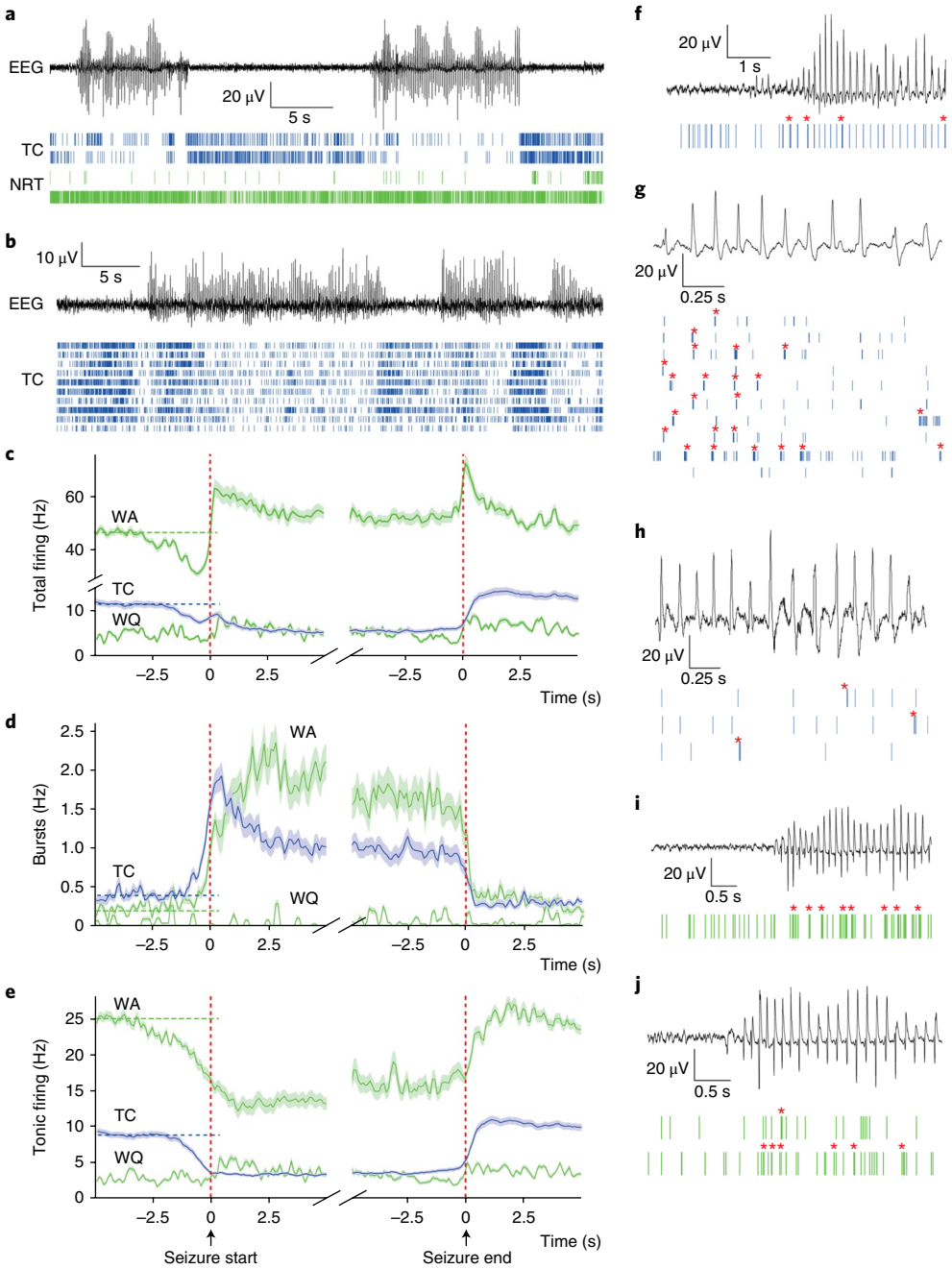

Fig. 2 | Temporal dynamics of TC and NRT neuron ensemble firing during ASs in GAERS rats. a, Spike-time raster plots (bottom traces) from two TC (blue) and two NRT (green, top WQ, bottom WA) neurons with time-matched EEG (top trace) in a GAERS rat. Note the sparse firing of TC neurons during ASs and the diverse firing of the two NRT neurons. **b**, Spike-time raster plots (bottom traces) from ten TC neurons with time-matched EEG (top trace) in another GAERS rat. Note the decrease in TC neuron firing during ASs. (**c**–**e**) Temporal evolution of total (**c**), burst (**d**) and tonic (**e**) firing before, during and after ASs for TC (blue) and NRT neurons (green) (lines: mean; shaded areas: ± s.e.m.) (n = 1,216 SWDs; n = 139 TC neurons; n = 13 WA and 12 WQ NRT neurons). Note the similar rate of increase (1.2 Hz/s) of bursts in TC and NRT neurons from about 1 s before SWD detection in the EEG. At the time of the peak of burst firing of TC neurons, NRT bursts continue to increase, but at a slower rate (0.5 Hz/s). Vertical red dashed lines indicate the start and end of SWDs in the EEG; horizontal dashed lines indicate mean pre-ictal firing rates. **f**–**j**, Spike-time raster plots (bottom traces) and time-matched EEG (top trace) for different TC and NRT neurons at interictal-to-ictal transitions (**f**,**i**,**j**), at the very start of an AS (**g**) and in the middle of an AS (**h**). Note the high prevalence of bursts (red asterisks) in TC and NRT neurons at the start of ASs.

only cortical burst firing (Fig. 6a) had a larger post-zero peak compared to those that included only tonic firing (Supplementary Fig. 10a) or total firing (Fig. 6a), indicating enhanced cortical to TC neuron excitation when cortical neurons fired bursts. Conversely, TC burst-firing XCors had almost no post-zero component (Fig. 6a), indicating that cortical excitation selectively drives TC neuron tonic firing. Moreover, XCors associated with the largest SWC spikes (the fourth quartile of amplitude) showed enhanced TC–cortex and cortex–TC excitation compared to those with smaller SWC spikes (the first quartile) (Fig. 6d,e and Supplementary Fig. 10b), indicating that TC and cortical neurons are more effectively recruited during cycles with higher cortical synchrony. Notably, the gain

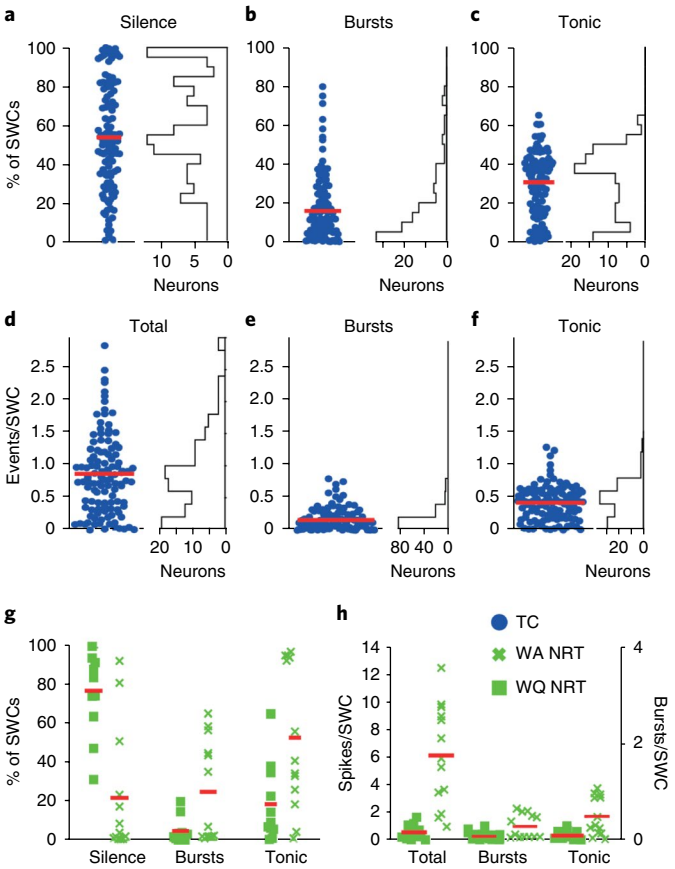

Fig. 3 | Ictal firing properties during ASs in GAERS rats. a–c, Electrical silence (**a**), bursts (**b**) and tonic (**c**) firing observed at each SWCs are plotted as percentage of SWCs for each TC neuron (left) and as distribution for the TC neuron population (right) ($n=139$). Twelve (9%) TC neurons were completely silent during ASs and 62 (45%) were silent for >50% of SWCs. Moreover, 33 (24%) TC neurons showed no burst during ASs, 84 (61%) neurons exhibited bursts for <20% of SWCs and no TC neuron had bursts for >80% of SWCs. (**d–f**) Number of events per SWC for total (**d**), bursts (**e**) and tonic firing (**f**) are plotted for each TC neuron (left) and as a distributions for the TC neuron population (right) ($n=139$ neurons). **g**, Same plots as in **a–c** for WA and WQ NRT neurons. **h**, Same plots as in **d**,**e** for WA and WQ NRT neurons. Red lines in **a–h** indicate mean values.

in strength of the cortex–TC interactions was higher than that of TC–cortex interactions (Fig. 6f), indicating that increased SWC-spike amplitude is accompanied by enhanced cortical (over thalamic) influence on network dynamics.

XCors of pairs of simultaneously recorded NRT and cortical neurons had only post-zero peaks for any type of firing, indicating a clear excitatory drive from cortical to NRT neurons, which was strongest when cortical neurons fired bursts (Fig. 6b) and elicited both tonic and burst firing in NRT neurons (Fig. 6b and Supplementary Fig. 10c). Notably, the probability of NRT neuron firing was higher in the 100 ms periods after a cortical than a TC neuron action potential, indicating that the cortex is a more significant source of ictal NRT excitation (Fig. 6c).

In summary, during ASs (i) bidirectional excitation occurs between cortical and TC neuron populations, (ii) cortical drive preferentially elicits tonic and not burst firing in TC neurons, and (iii) cortical firing is evoked by both tonic and burst firing of TC neurons. Finally, the presence of stronger excitatory drive from cortex to NRT neurons than from TC to NRT neurons suggests that the intrathalamic inhibition recruited ictally (Fig. 5a–c) most likely represents a cortex-dependent feedforward mechanism.

TC neuron T-channels do not contribute to ictal thalamic output synchrony. Since the above results do not support a thalamo-cortical pacemaker mechanism involving TC neuron T-channel-mediated burst firing[7,10,11,13], we directly tested the contribution of these channels to the ictal TC neuron output. T-channels were blocked by administration of the selective antagonist TTA-P2[27] via reverse microdialysis unilaterally into the VB of freely behaving GAERS rats while simultaneously recording single TC neuron activity from an adjacent silicon probe. TTA-P2 (300 µM in the inlet dialysis probe) abolished high-frequency bursts in all recorded TC neurons ($n=7$) during ASs as well as sleep, but tonic firing persisted during ASs and wakefulness, though reduced by 57 ± 6% of pre-drug rates during seizures ($P = 0.031$) (Fig. 7a,b). Following TTA-P2-elicited block of bursts, TC neuron total and tonic firing distributions expressed peaks with similar strength of phase preference and time relative to the SWC spike as before antagonist application ($n=7$, $P= 0.843$) (Fig. 7c,d). These data demonstrate that TC neurons are capable of delivering strong synchronous output to the neocortex during ASs even when their T-channels (and burst firing) are fully blocked and, notably, that these channels are not required for dictating the ictal firing time of TC neurons.

Cortical and NRT but not TC neuron T-channels are essential for ASs. Though the above results indicate that TC neuron T-channels are not necessary for the synchronized ictal thalamic output to neocortex, they do not obviate a critical role for these channels in ASs. Thus, we next applied TTA-P2, bilaterally this time, by reverse microdialysis in freely moving GAERS rats using a method that had established the spatio-temporal profile of TTA-P2-mediated full block of thalamic T-channels[28] (Methods). Specifically, our microdialysis dose–response and time–response analyses[28] showed that TTA-P2 applied at a concentration of 300 µM from a probe positioned in the center of the VB abolishes (in ~20 min) T-channel bursts within a volume that entirely encompasses this thalamic nucleus without affecting NRT neuron T-channels. Blocking T-channels throughout the VB with 300 µM TTA-P2 in eight GAERS rats using the above protocol did not affect ASs (Fig. 7e,f and Supplementary Fig. 11). In contrast, extending the block of T-channels to the NRT in six other GAERS rats by increasing TTA-P2 concentration (and thus affected tissue volume[28]) to 1 mM decreased ASs (Fig. 7e,f). Since in the latter experiment TTA-P2 would have also spread medially to the posterior nucleus, we then administered 300 µM TTA-P2 750 µm laterally from the center of the VB in six other GAERS rats, thus affecting the NRT and avoiding the posterior nucleus. In this case as well, the number and total duration of ASs were decreased by 50% (Fig. 7e,f and Supplementary Fig. 11). In a different group of GAERS rats ($n=9$), we inserted the probe 750 µm more medially from the center of the VB, thus fully avoiding the spread of TTA-P2 into the NRT. In this case, 1 mM TTA-P2 had no effect on ASs (Fig. 7e,f and Supplementary Fig. 11).

Recent studies showing that brain-wide genetic knockout or enhancement of CaV3.1 channels (the main T-channel subtype present in TC neurons[29]) abolishes[30] or induces[31] ASs, respectively, have been interpreted as suggesting a necessary role of TC neuron T-channels. Since CaV3.1 channels are also heavily expressed in neocortex[29], we tested the effect on ASs of their antagonism by TTA-P2 in the latter region. TTA-P2 (1 mM) applied by bilateral microdialysis in the S1pO (the initiation site of genetic rat SWDs[22,23]) of 16 GAERS rats decreased ASs by 36% (Fig. 7b and Supplementary Fig. 11).

Together with T-channel-mediated burst firing, $GABA_B$ receptors of TC neurons were suggested to be a key determinant of the temporal dynamics of TC neuron firing that underlie ictal thalamic

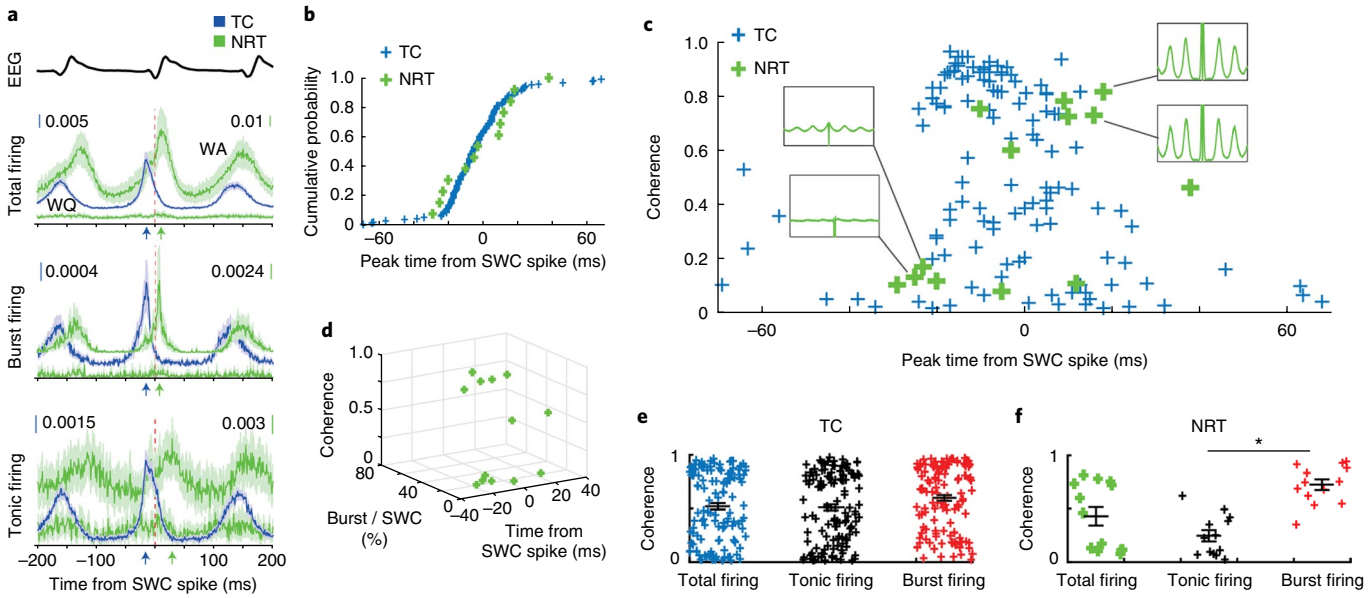

Fig. 4 | Synchrony and coherence of TC and NRT neuron firing during ASs. a, SWC-spike-triggered averages (lines: mean; shaded areas: ± s.e.m.) of total, burst and tonic firing for GAERS TC ($n=139$ in all panels), WA ($n=13$ in all panels) and WQ ($n=12$) NRT neurons. Note the different peak times (color-coded arrows) of TC and NRT neurons relative to SWC spike (red vertical line). Units are events per millisecond. **b**, Cumulative probability distributions of peak time of total firing for individual TC (blue) and WA NRT (green) neurons show no statistical difference between the two neuronal populations ($P=0.631$; Kolmogorov–Smirnov test). **c**, SWC coherence of total firing vs. peak time of total firing for individual GAERS TC and WA NRT neurons. Note the high coherence for TC neurons with peak firing times between −20 and 0 ms. In contrast, NRT neurons show low coherence (and flat autocorrelograms, left green insets) when their firing peaks occur in the −20 to 0 ms interval but high coherence (and clear peaks in the autocorrelograms, right green insets) when their firing peaks is after 0 ms. **d**, 3D plot showing that NRT neurons with high coherence have a relatively high burst rate and fire relatively late with respect to the SWC spike while those NRT neurons with low coherence have a relatively low burst rate and fire early with respect to the SWC spike. **e**,**f**, SWC coherence for different firing types (mean ± s.e.m. in black) for individual TC (**e**) and NRT (**f**) neurons. Note the higher coherence of burst vs. tonic firing in NRT neurons (*$P=7\times10^{-5}$, $n=13$ neurons, two-sided signed rank test).

rhythmogenesis and determine SWD frequency[10,12,13]. Thus, we next investigated the effect of bilateral microdialysis (in the center of the VB) of the $GABA_B$ antagonist CGP55845 at submaximal concentration (500 μM). This drug markedly suppressed the total time spent in ASs (artificial cerebrospinal fluid control (aCSF): 87.0 ± 18.3%; CGP55845: 5.69 ± 1.4% of pre-drug control, $n=10$ GAERS rats, $P=0.0156$, Wilcoxon paired signed-rank two-sided test), as previously shown for other $GABA_B$ antagonists[8,19], but had no effect on the frequency of the SWDs of the remaining seizures (aCSF: 6.88 ± 0.1 Hz; CGP55845: 6.74 ± 0.1 Hz, $P=0.5781$, $n=7$, Wilcoxon paired signed-rank two-sided test). In summary, these results demonstrate that T-channels of NRT and cortical, but not TC, neurons are necessary for the expression of behavioral ASs.

Top-down excitation enables ictal TC neuron recruitment in the absence of burst firing. To test the neuronal mechanism of thalamic firing during ASs suggested by the experimental results, we used a simple biophysical network model (Fig. 8a, Supplementary Table 3 and Methods). It includes one TC neuron that is connected via $GABA_A$ synapses alone to two NRT neurons, one that preferentially fires bursts and one that has both tonic and burst firing (compare Fig. 3g) due to a more depolarized membrane potential (Fig. 8a,b). Two cortical pyramidal neurons are connected to the NRT neurons, and reciprocally to the TC neuron, via AMPA synapses (Fig. 8a). Simulations were driven by trains of five excitatory postsynaptic potentials (EPSPs) delivered to the cortical neurons alone at 7 Hz (Fig. 8a,b), i.e., the frequency of GAERS SWDs[19].

The model (Supplementary Fig. 12a) reproduced the TC and NRT neuron firing distributions observed experimentally (Fig. 4a). Notably, the firing peak of the more depolarized NRT neuron occurred earlier than that of the NRT neuron that preferentially fired bursts (Supplementary Fig. 12a) and was coincident with the TC neuron peak firing when NRT–TC synapses were blocked (Supplementary Fig. 12c). Moreover, increasing the strength of TC–NRT synapses (up to sixfold higher than the cortex–NRT synapses) did not affect the firing distribution (Supplementary Fig. 12b). By contrast, removing cortical-to-NRT synapses (Supplementary Fig. 12f) or T-channels in NRT neurons (Supplementary Fig. 12h) resulted in deviation of the distributions from both the simulated control conditions (Supplementary Fig. 12a) and the experimental results (Fig. 4a). Furthermore, removing inhibitory NRT-to-TC synapses significantly broadened the peak of the TC firing distribution ($k=2.03$ vs. $k=3.59$, $P<0.001$; Kuiper test) (Supplementary Fig. 12c), supporting the sharpening effect of NRT inhibition on thalamic output.

XCors of the simulated firing closely reproduced those observed experimentally, notably in the presence of a trough in TC–NRT XCors (compare Figs. 8c and 5a) and in the occurrence of two peaks in the TC–cortex XCors (compare Figs. 8c and 6a). Similarly to the simulated firing distributions, the various XCors were not qualitatively affected by a large increase in TC-to-NRT synapse strength (compare Figs. 8c and 8d) or removal of TC T-channels (Fig. 8i). As expected, removing TC-to-cortex (Fig. 8f) or cortex-to-TC (Fig. 8g) synapses abolished the peak before or after time zero, respectively. Removing NRT-to-TC inhibition (Fig. 8e), cortex–NRT excitation (Fig. 8h) or NRT T-channels (Fig. 8j) also generated XCors lacking key features of simulated control conditions and experimental results: the post-zero trough in TC–NRT, the post-zero peak in NRT–cortex and the narrow peaks in all XCors, respectively. In summary, these simulations confirmed that (i) fast $GABA_A$-mediated NRT-to-TC inhibition is sufficient to sharpen TC neuron ictal firing, (ii) a strong TC-to-NRT excitatory connection is not required to explain the ictal firing of NRT neurons, and

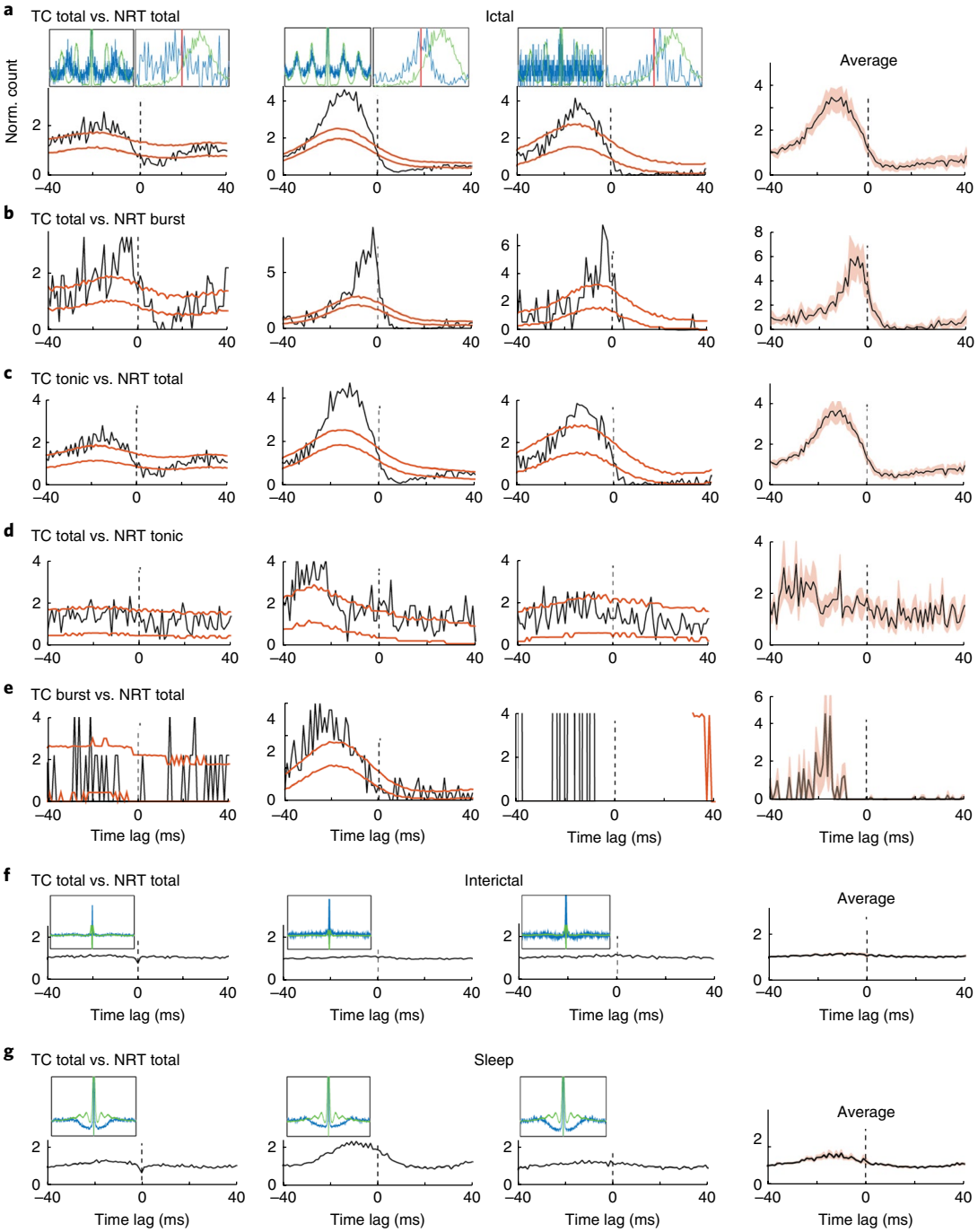

Fig. 5 | Ictal recruitment of NRT–TC neuron inhibitory assemblies. a–**g**, Representative XCors (black trace) of firing of three representative pairs of simultaneously recorded TC and NRT neurons (three leftmost columns) (brown lines indicate expected 5–95% confidence intervals estimated from surrogate firing time trains for each neuron in its respective firing distribution relative to the SWC; see Methods). The average XCors (black line; red shadow: ± s.e.m.) of five pairs is shown in the rightmost column. The significant (below confidence interval) troughs after 0 ms in the XCors indicates a lower probability of the TC neuron firing after an NRT spike (**a**), which is maintained when NRT burst firing (**b**) or TC tonic firing (**c**) is used for the analysis. No statistically significant sharp peak or trough is present when NRT tonic firing (**d**) or TC burst firing (**e**) is used. The same three pairs do not exhibit these peaks or troughs during interictal periods (**f**) and non-REM sleep (**g**). Top left insets in **a**,**f**,**g** show superimposed autocorrelograms for the respective TC (blue) and NRT (green) neurons calculated between −400 and 400 ms from the SWC spike. Top right insets in **a** show superimposed spike distribution of the respective TC (blue) and NRT (green) neuron calculated from −40 to 40 ms of the SWC spike (red lines). For both insets, each curve maximum amplitude is normalized to 1.

(iii) bidirectional excitation between TC and cortical neurons coupled with cortical drive of NRT neurons can explain the experimentally observed ictal interactions between the two thalamic neuronal populations and among cortical and thalamic neuronal assemblies.

Discussion

Neuronal ensemble activity of single thalamic and cortical neurons demonstrates synchronous bidirectional cortico-thalamo-cortical communication during ASs in behaving animals. The cortical and

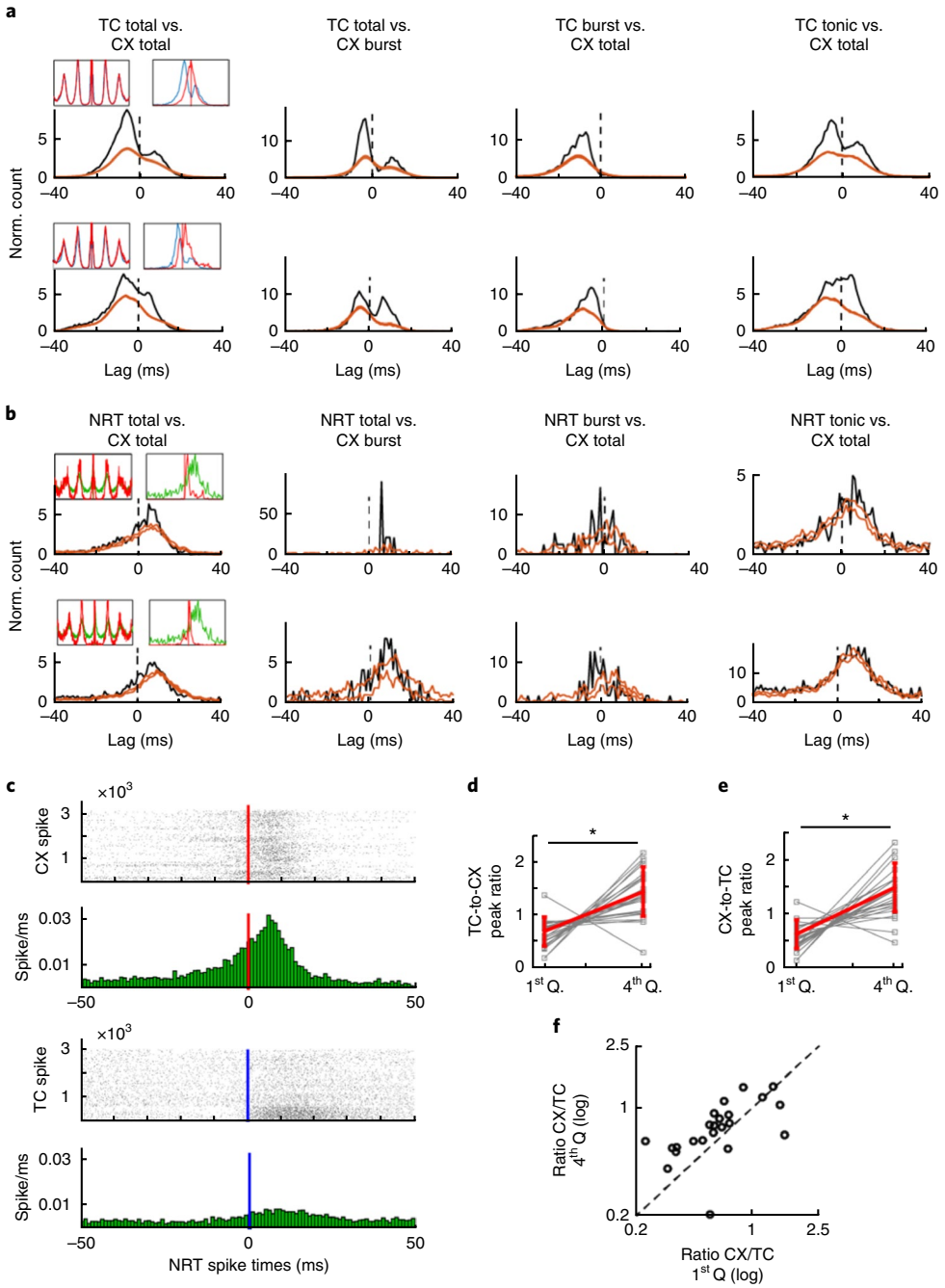

Fig. 6 | Ictal cortical drive of thalamic neuronal populations. a, Representative XCors (black trace) of firing of two representative pairs of simultaneously recorded TC and cortical (CX) neurons (brown lines indicate expected 5–95% confidence intervals estimated as described in Fig. 5). The presence of two peaks, one before and one after time zero, which are more evident when only CX neuron bursts were used for the analysis, indicates reciprocal excitation between TC and CX neurons. Top left insets show superimposed autocorrelograms for the respective TC (blue) and CX (red) neurons calculated between −400 and 400 ms from the SWC spike. Top right insets show superimposed spike distribution of the respective TC (blue) and CX (red) neuron calculated from −40 to 40 ms with respect to the SWC spike (red lines). For both insets, each curve maximum amplitude is normalized to 1. **b**, Representative XCors as in **a** but for two representative pairs of simultaneously recorded NRT and CX neurons. The significant peak after time zero indicates the increased probability of NRT neuron firing following CX firing. Note that this peak is much larger and sharper when only CX burst firing is used for the analysis. Top left and right insets in **b** are as in **a** but for NRT (green) and CX (red) neurons. **c**, Peri-spike raster plots (top graphs) and histograms (bottom graphs) of NRT firing with respect to CX and TC neuron spike occurring at time 0 (red and blue line, respectively), calculated from simultaneously recorded CX–NRT and TC–NRT pairs. In the histograms, note the clear peak (sixth bin after time zero) following CX but not TC neuron firing (horizontal red and blue line, respectively). **d**, Ratio of the XCors peaks (lines: mean; error bars: ± s.e.m.) of TC-to-CX interaction (i.e., peak before time zero) for the first and fourth quartiles (Q) of SWC-spike amplitudes over peaks for all SWC-spike amplitudes (Supplementary Fig. 10b and Methods) ($^*P = 1.26 \times 10^{-4}$, one-sided signed rank test, $n = 25$ independent pairs of TC–CX neurons). **e**, Same plot as **d** for the XCors peak of CX-to-TC interactions (i.e., peak after time zero) ($^*P = 3.04 \times 10^{-5}$, one-sided signed rank test, $n = 25$ pairs of neurons). **f**, Ratio of CX–TC and TC–CX peaks for the highest versus the lowest SWC-spike amplitude quartile indicate a gain of cortico-thalamic over the thalamo-cortical contribution to the XCors ($P = 8.3 \times 10^{-3}$, one-sided signed rank test, $n = 25$ neuron pairs) for the largest SWC spike.

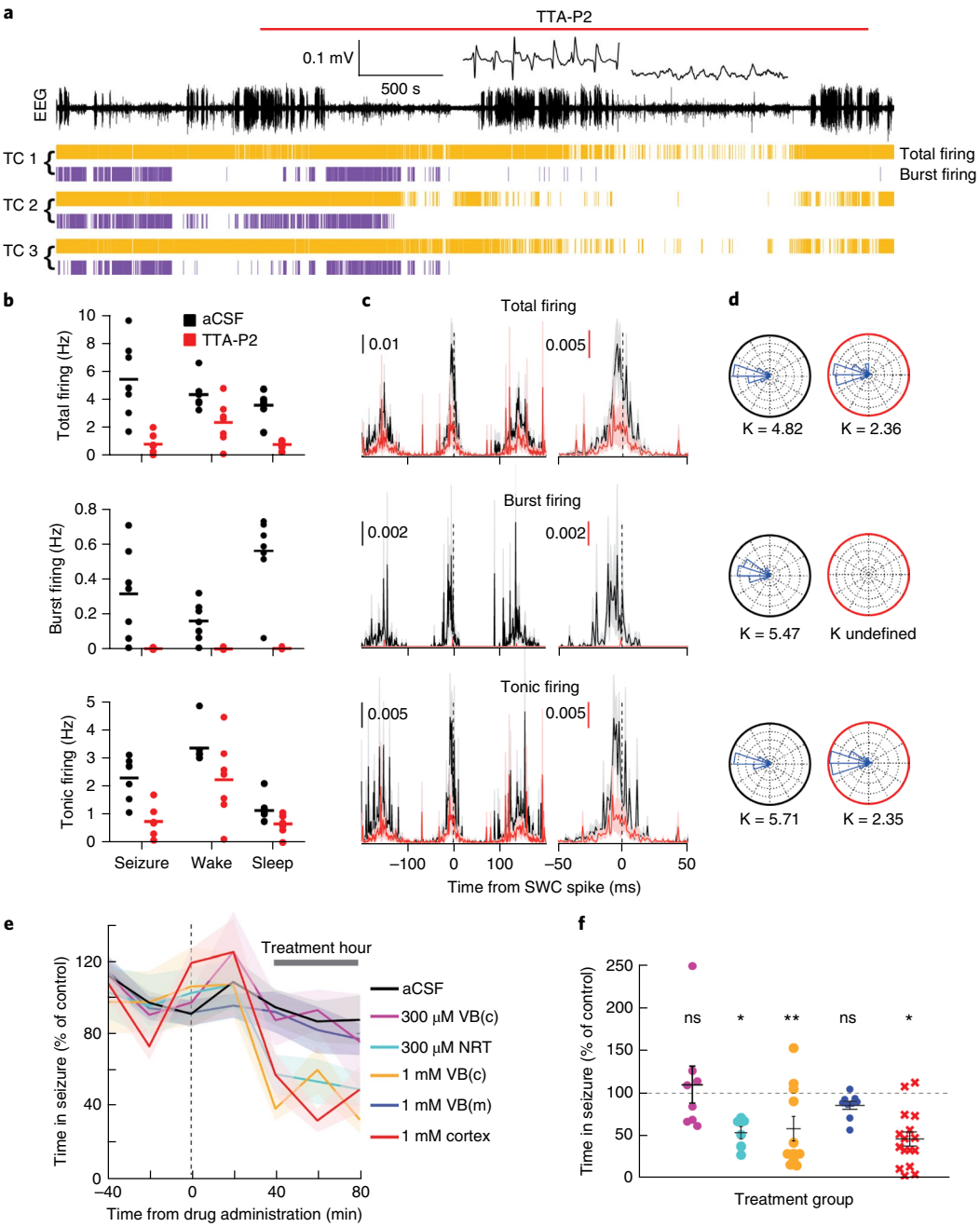

Fig. 7 | Block of T-channels in NRT and S1pO cortex markedly reduces ASs whereas block in TC neurons does not affect thalamic output synchrony or behavioral ASs. a, EEG (top trace), and spike-time (yellow) and burst-time (violet) raster plots (bottom traces) from three simultaneously recorded TC neurons in VB of a GAERS rat before and during reverse microdialysis administration of 300 µM TTA-P2 (marked by red line) from an adjacent microdialysis probe. Note the complete block of bursts by TTA-P2 during both ASs and sleep periods (enlarged left and right trace, respectively, at the top of the EEG record). **b**, Rates of different firing types before (black) and during (red) complete block of bursts by TTA-P2 show decrease in total ($P=0.016$), burst ($P=0.016$) and tonic ($P=0.031$) firing during ASs, and in total ($P=0.031$) and burst ($P=0.016$) but not tonic ($P=0.16$) firing during wakefulness (paired two-sided Wilcoxon signed-rank test). Horizontal lines indicate the mean of $n=7$ TC neurons. **c**, SWC-triggered means of different firing types (total, burst, tonic) of $n=7$ TC neurons show clear peaks near the EEG SWC spike (indicated by the vertical black dashed line) before (black) and during (red) complete block of bursts by TTA-P2. Shaded areas indicate ± s.e.m. Units are events per millisecond. **d**, Circular firing distribution and mean circular concentration coefficient (κ) showing similar value before (black circles) and during (red circles) TTA-P2 administration ($n=7$ independent neurons, $P=0.843$, paired two-sided Wilcoxon signed-rank test; κ undefined for burst firing during TTA-P2 dialysis because bursts were completely abolished). **e**, Time course of total time in seizure before and during bilateral thalamic reverse microdialysis of aCSF or different concentrations of TTA-P2 in GAERS rats (lines and shaded areas: mean ± s.e.m.; treatment hour indicates the period analyzed in **f**). Black dashed vertical line indicates the start of TTA-P2 dialysis. $n=8$ GAERS rats with 300 µM TTA-P2 in the center of the VB (VB(c)), 11 with 1 mM TTA-P2 in VB(c), 6 with 300 µM in NRT, 9 with TTA-P2 medial to the center of the VB (VB(m)) and 16 with 1 mM TTA-P2 in S1pO cortex. Microdialysis of 1 mM TTA-P2 in VB(c) blocks bursts both in VB and NRT[28]. **f**, Mean total time spent in seizure by GAERS rats during different TTA-P2 applications (n as in **e**) was calculated during the treatment hour as a percentage of that in the control hour (before TTA-P2 administration) (colors as in **e**; black horizontal lines: mean ± s.e.m., $P=0.7422$, 0.0313, 0.0186, 0.7344, 0.0182, paired two-sided Wilcoxon signed-rank test). The effect of TTA-P2 on number and duration of ASs and on SWD frequency is illustrated in Supplementary Fig. 12.

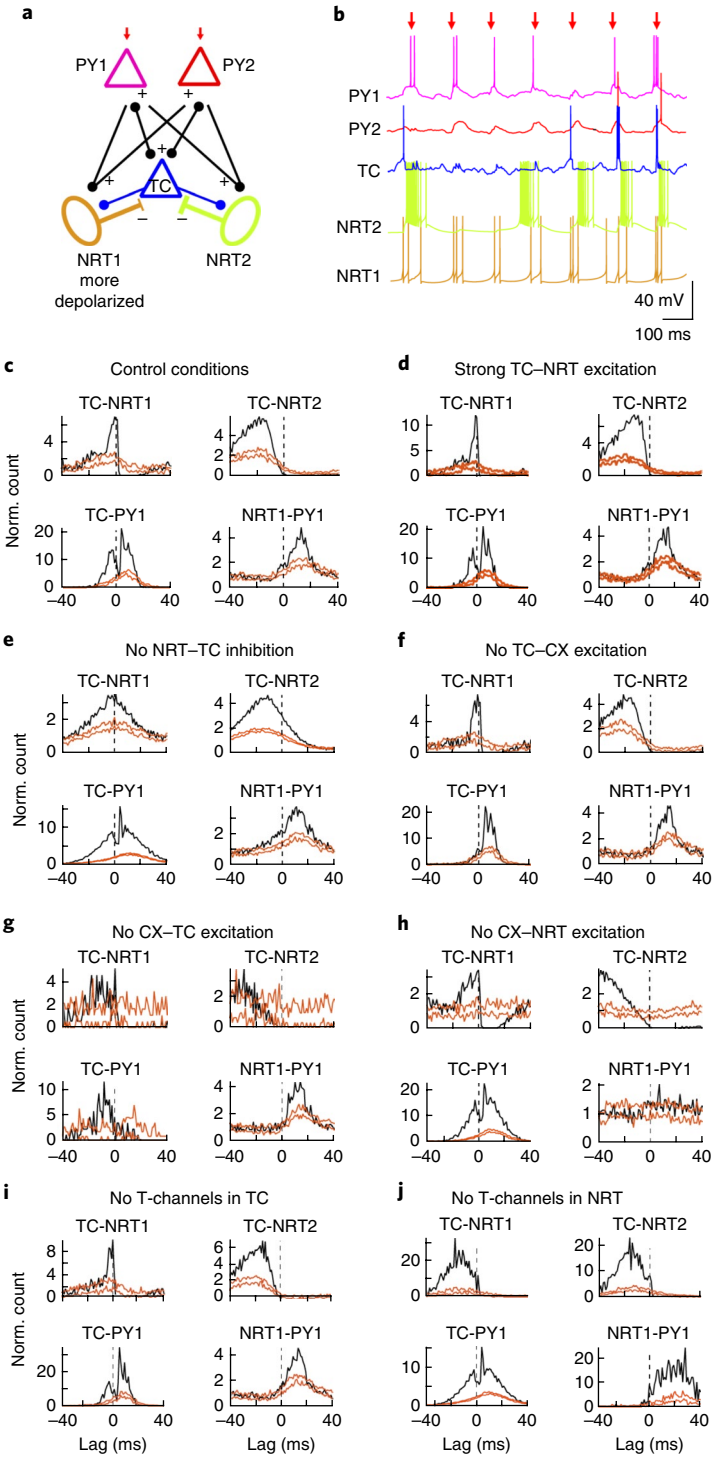

Fig. 8 | Firing interactions in a cortico-thalamic network model. a, Diagram of the model network, consisting of 1 TC, 2 NRT and 2 excitatory cortical pyramidal (PY) neurons. NRT1 is more depolarized than NRT2 by steady injected current. Excitatory (AMPA) synapses connect TC to NRT and PY neurons, and PY neurons to NRT and TC neurons. Inhibitory $GABA_A$ synapses connect NRT to TC neurons. Only PY neurons receive a train of 5 AMPA EPSPs that is repeated at a frequency of 7 Hz. Red arrows indicate the third EPSP in the train, which was used as time reference for the analysis. **b**, Example membrane potential traces illustrate the firing dynamics during the 7-Hz stimulation protocol. Note the presence of high-frequency bursts in NRT2 and their paucity in TC and NRT1 neuron. **c**–**j**, XCors (black) of simulated firing of different neuron pairs under various conditions (brown lines indicate expected 5–95% confidence intervals estimated as in Fig. 5 using the third EPSPs as a time reference). The simulation under control conditions well reproduced the experimental XCors (**c**), and no major change was observed in simulations with an increase in the strength of the TC-to-NRT neuron synapse up to sixfold that of the cortex–NRT neuron synapses (**d**), whereas blocking the NRT-to-TC neuron $GABA_A$ synapses abolished the trough after time zero in TC–NRT neuron XCors (**e**). Block of cortical-to-TC neuron synapses or vice versa led to TC–cortex XCors that were different from those observed experimentally (**f**,**g**), and while a trough was still present in TC–NRT XCors when the cortical input to NRT neurons was absent, there was no peak in NRT–cortex XCors (**h**). Removal of T-channels in TC neurons had no major effect on the XCors (**i**), whereas in NRT neurons it led to broader XCors peaks (**j**) compared to the control conditions (**a**).

NRT components of this activity are T-channel dependent and required for AS expression. The TC neuron population contributes synchronous volleys of firing, mainly tonic, that are driven by cortical excitation and framed by NRT-mediated inhibition, mainly feedforward.

Thalamic firing dynamics. The disagreements between our findings and previous studies indicate that the use of brain slices[10,11] or anesthetized or fentanyl conditions[14–16,23] results in different TC and NRT neuron ictal firing dynamics than those of behavioral ASs. Specifically, our results show that during ASs total firing of TC neurons is markedly decreased, as well as temporally framed within each SWD cycle, and that the synchrony and strength of TC ictal output to the neocortex is not a feature of single, rhythmically bursting TC neurons but is an emergent property of this population, as suggested originally by Buzsáki[32]. This contrasts with the conclusions of a recent study[33], in which behavioral ASs were induced and suppressed by switching TC firing between a rhythmic and nonrhythmic mode, respectively, with the former mode's synchrony being indirectly attributed to T-channel-dependent bursts on the basis of in vitro optogenetic experiments. Although the significance of thalamic synchrony to ASs is not contradicted by our present work, the cellular or synaptic cause of that synchrony would not have been detectable at the level of multi-unit activity used by Sorokin et al.[33]. Furthermore, even if one were to assume that TC neuron T-channel-dependent bursts were responsible for that study's induction of ASs, this does not imply that they are an inevitable and necessary component of the paroxysmal oscillation. In fact, when single-cell resolution is achieved, as in our current work, ictal thalamic output synchrony is shown to be reliant not on T-channels, but rather on excitation and feedforward inhibition of cortical origin.

The ictal reduction of total firing in TC neurons of both GAERS and GHB models may result from their increased tonic $GABA_A$ inhibition[34,35]. Such increased tonic $GABA_A$ inhibition has also been shown to prolong the decay of $GABA_A$ inhibitory postsynaptic potentials (IPSPs) evoked in TC neurons by NRT-neuron single action potentials or bursts[36], which could explain the ability of NRT burst-induced IPSPs to completely suppress TC output through most of the SWD cycle. Considering that tonic inhibition provides 90% of $GABA_A$ inhibition in TC neurons[37], the gain of function of TC-neuron extrasynaptic $GABA_A$ receptors in epileptic animals[34] is sufficient to explain the electrical silence, the marked decrease of tonic firing and the paucity of rebound bursts observed ictally in GAERS TC neurons. This, in turn, may provide the thalamic basis for the decreased response to sensory stimulation during ASs[8,9].

The peak in TC neuron burst firing at the start of ASs may result from the time-dependent plasticity that is known to occur at both excitatory cortex–TC and inhibitory NRT–TC synapses: optogenetic stimulation of cortico-thalamic afferents at 10 Hz (a frequency similar to that of rodent SWDs) initially evokes in VB TC neurons a synaptic sequence of a small inward–large outward current, which transforms into a stable large inward–small outward current within the first second of stimulation[38].

Role of T-channels. Our findings question the view that TC neuron burst firing is critical for ASs[7,10,12,13]. First, the unaltered synchrony of ictal thalamic output to the neocortex during a block of TC burst firing demonstrates that these channels do not determine SWD frequency, as was previously proposed[7,10,11]. The lack of effect on SWD frequency of blocking $GABA_B$ receptors in TC neurons further contradicts the mechanistic hypothesis in which synaptic $GABA_B$ receptor current and cell-intrinsic T-channel current interact to determine the timing of TC neuron firing and thus SWD frequency[10,12,13]. The partial block of thalamic tonic firing output by TTA-P2 may be explained by the small but significant contribution of T-channels to tonic firing and the input–output function of TC neurons at depolarized membrane potentials because of the physiologically significant fraction of T-channels that are de-inactivated at these potentials[39]. However, we cannot exclude the possibility that some single spikes included in our tonic firing classification may be generated by a low-threshold spike.

Second, the lack of effect on ASs of TTA-P2 applied in the VB demonstrates that T-channels of this nucleus, somatotopic to the cortical initiation site[22,23], are not required for the expression and maintenance of these seizures. By contrast, sleep spindles, a cortico-thalamo-cortical network oscillation with a well-established thalamic rhythmogenesis[5,6], are abolished when T-channels of VB TC neurons are blocked by an identical TTA-P2 microdialysis application[28] as in the current work.

Notably, the reduction in ASs following the block of T-channels in cortical neurons indicates that bursts in the neocortex (and possibly other regions, which could include nonsensory thalamic nuclei) underlie the effects on ASs following brain-wide genetic manipulations of CaV3.1 channels[30,31]. Meanwhile, the marked reduction in ASs following the block of NRT neuron T-channels confirms that CaV3.2 and/or CaV3.3 channels, the two T-channel subtypes present in these neurons[29], play a key role in genetically determined ASs, as indicated by CaV3.2 channel mutations in GAERS NRT neurons[40] and human absence epilepsy cohorts[41]. Notably, however, GHB-induced ASs are resistant to the knockout of both CaV3.2 and CaV3.3 channels[42].

Ictal cortico-thalamo-cortical interactions. Our results provide direct evidence that NRT–TC inhibitory short-term assemblies become engaged ictally in a manner that is critically dependent on NRT bursts and fast $GABA_A$ synapses. This is indicated by the lack of NRT–TC inhibition in XCors that considered only NRT neuron tonic firing, as well as the close similarity between experimental XCors of TC and NRT neuron ictal firing and those simulated using only $GABA_A$ synapses. Thus, fast NRT inhibition frames ictal TC neuron firing, and the higher coherence of NRT neuron burst firing that occurs just after the SWC spike is likely to reflect sharpening of the TC neuron response by these bursts.

The lack of a sharp peak in TC–NRT neuron XCors does not suggest an ictal, strongly active monosynaptic connection between TC and NRT neuron pairs, and modeled ictal firing and interactions were not altered by varying TC–NRT synapse strength. This absence of a major involvement of TC–NRT excitatory synapses during ictal firing interactions may be an unexpected finding, since this connection has been reported to be strong and reliable in juvenile rats[43]. However, in adult animals tonic TC neuron firing at 40 Hz evokes only small EPSPs in NRT neurons, whereas TC bursts evoke larger NRT EPSPs[44]. In view of this, and of our observed ictal 6-Hz tonic and 1-Hz burst firing rates, relatively weak (but not absent) ictal TC–NRT compared to cortex–NRT excitation is not surprising. Indeed, optogenetic stimulation of cortico-thalamic afferents is not highly effectively in activating the TC-to-NRT pathway in vitro[45], supporting the lower probability of ictal NRT firing following TC than cortical neuron firing that we observed.

In summary, our findings show that ASs do not rely on widespread TC neuron bursts but rather on cortico-thalamic inputs exciting both TC and NRT neurons and on thalamic feedforward inhibition. Thus, the most parsimonious mechanism of a SWD cycle involves reciprocal excitation of TC and cortical neurons, as well as excitation of NRT neurons mainly by cortico-thalamic neurons. The precise timing of this excitation may depend on intracortical rhythmogenic mechanisms, as well as cortico-thalamic interactions. NRT neuron firing then temporally frames TC neuron output by suppressing firing throughout most of the spike-wave cycle. The framed TC output may help to re-engage and synchronize the cortex in the next cycle, but rebound bursts are not a

necessary part of this output, contrasting with thalamic slice and in silico models[7,10–13]. In other words, the temporal precision of TC neuron ictal firing is not dictated by the interaction of T-channel activation/inactivation and $GABA_A$/$GABA_B$ IPSP dynamics[10,12,13] but rather by the interplay of excitatory cortico-thalamic and fast feedforward NRT inhibitory drives, which are known to shape cortico-thalamo-cortical activity in other behavioral contexts[38,45,46]. On the other hand, the interplay of cortico-thalamic input and cell-intrinsic mechanisms (including T-current and Ca^{2+}-activated currents[9]) underlies NRT neuron ictal excitation.

Significance for human ASs. The strong similarities in firing dynamics and neuronal interactions of ASs between a polygenic (GAERS) and a pharmacological (GHB) model suggest that similar mechanisms may underlie generalized non-convulsive seizures in other models with spontaneous or induced single-gene mutations[47]. Nevertheless, selective impairment of cortex-to-NRT transmission, leading to a reduction of feedforward inhibition of TC neurons, can induce ASs[48], and it would be of interest to investigate the ictal mechanism of human $GABA_A$ γ2R43Q knock-in mice that, in contrast to the GAERS and GHB models, have decreased tonic $GABA_A$ inhibition in TC neurons[49]. These different models undoubtedly offer insights into the mechanisms underlying the large diversity in SWD waveform and AS severity encountered in childhood and juvenile absence epilepsies[50].

Methods

Methods, including statements of data availability and any associated accession codes and references, are available at https://doi.org/10.1038/s41593-018-0130-4.

Received: 17 January 2018; Accepted: 8 March 2018;
Published online: 16 April 2018

References

1. McCormick, D. A. & Bal, T. Sleep and arousal: thalamocortical mechanisms. *Annu. Rev. Neurosci.* **20**, 185–215 (1997).
2. Crunelli, V. & Hughes, S. W. The slow (1 Hz) rhythm of non-REM sleep: a dialogue between three cardinal oscillators. *Nat. Neurosci.* **13**, 9–17 (2010).
3. Schmitt, L. I. et al. Thalamic amplification of cortical connectivity sustains attentional control. *Nature* **545**, 219–223 (2017).
4. Steriade, M., Jones, E. G. & McCormick, D. A. *Thalamus – Organisation and Function* Vol. 1 (Elsevier Science, New York, 1997).
5. Crunelli, V. et al. Dual function of thalamic low-vigilance state oscillations: rhythm-regulation and plasticity. *Nat. Rev. Neurosci.* **19**, 107–118 (2018).
6. Contreras, D. & Steriade, M. Spindle oscillation in cats: the role of corticothalamic feedback in a thalamically generated rhythm. *J. Physiol.* **490**, 159–179 (1996).
7. McCormick, D. A. & Contreras, D. On the cellular and network bases of epileptic seizures. *Annu. Rev. Physiol.* **63**, 815–846 (2001).
8. Crunelli, V. & Leresche, N. Childhood absence epilepsy: genes, channels, neurons and networks. *Nat. Rev. Neurosci.* **3**, 371–382 (2002).
9. Blumenfeld, H. Cellular and network mechanisms of spike-wave seizures. *Epilepsia* **46** (Suppl. 9), 21–23 (2005).
10. von Krosigk, M., Bal, T. & McCormick, D. A. Cellular mechanisms of a synchronized oscillation in the thalamus. *Science* **261**, 361–364 (1993).
11. Huntsman, M. M., Porcello, D. M., Homanics, G. E., DeLorey, T. M. & Huguenard, J. R. Reciprocal inhibitory connections and network synchrony in the mammalian thalamus. *Science* **283**, 541–543 (1999).
12. Destexhe, A. Spike-and-wave oscillations based on the properties of $GABA_B$ receptors. *J. Neurosci.* **18**, 9099–9111 (1998).
13. Destexhe, A. *Neuronal Networks in Brain Function, CNS Disorders, and Therapeutics* 11–35 (Elsevier, New York, 2014).
14. Pinault, D. et al. Intracellular recordings in thalamic neurones during spontaneous spike and wave discharges in rats with absence epilepsy. *J. Physiol. (Lond.)* **509**, 449–456 (1998).
15. Steriade, M. & Contreras, D. Relations between cortical and thalamic cellular events during transition from sleep patterns to paroxysmal activity. *J. Neurosci.* **15**, 623–642 (1995).
16. Slaght, S. J., Leresche, N., Deniau, J.-M., Crunelli, V. & Charpier, S. Activity of thalamic reticular neurons during spontaneous genetically determined spike and wave discharges. *J. Neurosci.* **22**, 2323–2334 (2002).
17. Inoue, M., Duysens, J., Vossen, J. M. H. & Coenen, A. M. L. Thalamic multiple-unit activity underlying spike-wave discharges in anesthetized rats. *Brain Res.* **612**, 35–40 (1993).
18. Inoue, M., Ates, N., Vossen, J. M. H. & Coenen, A. M. L. Effects of the neuroleptanalgesic fentanyl-fluanisone (Hypnorm) on spike-wave discharges in epileptic rats. *Pharmacol. Biochem. Behav.* **48**, 547–551 (1994).
19. Depaulis, A., David, O. & Charpier, S. The genetic absence epilepsy rat from Strasbourg as a model to decipher the neuronal and network mechanisms of generalized idiopathic epilepsies. *J. Neurosci. Methods* **260**, 159–174 (2016).
20. Taylor, H. et al. Investigating local and long-range neuronal network dynamics by simultaneous optogenetics, reverse microdialysis and silicon probe recordings in vivo. *J. Neurosci. Methods* **235**, 83–91 (2014).
21. Venzi, M., Di Giovanni, G. & Crunelli, V. A critical evaluation of the gamma-hydroxybutyrate (GHB) model of absence seizures. *CNS Neurosci. Ther.* **21**, 123–140 (2015).
22. Meeren, H. K. M., Pijn, J. P. M., Van Luijtelaar, E. L. J. M., Coenen, A. M. L. & Lopes da Silva, F. H. Cortical focus drives widespread corticothalamic networks during spontaneous absence seizures in rats. *J. Neurosci.* **22**, 1480–1495 (2002).
23. Polack, P.-O. et al. Deep layer somatosensory cortical neurons initiate spike-and-wave discharges in a genetic model of absence seizures. *J. Neurosci.* **27**, 6590–6599 (2007).
24. Hazan, L., Zugaro, M. & Buzsáki, G. Klusters, NeuroScope, NDManager: a free software suite for neurophysiological data processing and visualization. *J. Neurosci. Methods* **155**, 207–216 (2006).
25. Barthó, P. et al. Ongoing network state controls the length of sleep spindles via inhibitory activity. *Neuron* **82**, 1367–1379 (2014).
26. Halassa, M. M. et al. State-dependent architecture of thalamic reticular subnetworks. *Cell* **158**, 808–821 (2014).
27. Dreyfus, F. M. et al. Selective T-type calcium channel block in thalamic neurons reveals channel redundancy and physiological impact of $I_{Twindow}$. *J. Neurosci.* **30**, 99–109 (2010).
28. David, F. et al. Essential thalamic contribution to slow waves of natural sleep. *J. Neurosci.* **33**, 19599–19610 (2013).
29. Talley, E. M. et al. Differential distribution of three members of a gene family encoding low voltage-activated (T-type) calcium channels. *J. Neurosci.* **19**, 1895–1911 (1999).
30. Kim, D. et al. Lack of the burst firing of thalamocortical relay neurons and resistance to absence seizures in mice lacking α_{1G} T-type Ca^{2+} channels. *Neuron* **31**, 35–45 (2001).
31. Ernst, W. L., Zhang, Y., Yoo, J. W., Ernst, S. J. & Noebels, J. L. Genetic enhancement of thalamocortical network activity by elevating α1G-mediated low-voltage-activated calcium current induces pure absence epilepsy. *J. Neurosci.* **29**, 1615–1625 (2009).
32. Buzsáki, G. The thalamic clock: emergent network properties. *Neuroscience* **41**, 351–364 (1991).
33. Sorokin, J. M. et al. Bidirectional control of generalized epilepsy networks via rapid real-time switching of firing mode. *Neuron* **93**, 194–210 (2017).
34. Cope, D. W. et al. Enhanced tonic GAB_{AA} inhibition in typical absence epilepsy. *Nat. Med.* **15**, 1392–1398 (2009).
35. Connelly, W. M. et al. GA_BA_B receptors regulate extrasynaptic GAB_{AA} receptors. *J. Neurosci.* **33**, 3780–3785 (2013).
36. Herd, M. B., Brown, A. R., Lambert, J. J. & Belelli, D. Extrasynaptic GAB_{AA} receptors couple presynaptic activity to postsynaptic inhibition in the somatosensory thalamus. *J. Neurosci.* **33**, 14850–14868 (2013).
37. Cope, D. W., Hughes, S. W. & Crunelli, V. GAB_{AA} receptor-mediated tonic inhibition in thalamic neurons. *J. Neurosci.* **25**, 11553–11563 (2005).
38. Crandall, S. R., Cruikshank, S. J. & Connors, B. W. A corticothalamic switch: controlling the thalamus with dynamic synapses. *Neuron* **86**, 768–782 (2015).
39. Deleuze, C. et al. T-type calcium channels consolidate tonic action potential output of thalamic neurons to neocortex. *J. Neurosci.* **32**, 12228–12236 (2012).
40. Powell, K. L. et al. A Cav3.2 T-type calcium channel point mutation has splice-variant-specific effects on function and segregates with seizure expression in a polygenic rat model of absence epilepsy. *J. Neurosci.* **29**, 371–380 (2009).
41. Chen, Y. et al. Association between genetic variation of *CACNA1H* and childhood absence epilepsy. *Ann. Neurol.* **54**, 239–243 (2003).
42. Lee, S. E. et al. Rebound burst firing in the reticular thalamus is not essential for pharmacological absence seizures in mice. *Proc. Natl Acad. Sci. USA* **111**, 11828–11833 (2014).
43. Gentet, L. J. & Ulrich, D. Strong, reliable and precise synaptic connections between thalamic relay cells and neurones of the nucleus reticularis in juvenile rats. *J. Physiol. (Lond.)* **546**, 801–811 (2003).
44. Kim, U. & McCormick, D. A. The functional influence of burst and tonic firing mode on synaptic interactions in the thalamus. *J. Neurosci.* **18**, 9500–9516 (1998).
45. Cruikshank, S. J., Urabe, H., Nurmikko, A. V. & Connors, B. W. Pathway-specific feedforward circuits between thalamus and neocortex revealed by selective optical stimulation of axons. *Neuron* **65**, 230–245 (2010).

46. Mease, R. A., Krieger, P. & Groh, A. Cortical control of adaptation and sensory relay mode in the thalamus. *Proc. Natl Acad. Sci. USA* **111**, 6798–6803 (2014).
47. Maheshwari, A. & Noebels, J. L. Monogenic models of absence epilepsy: windows into the complex balance between inhibition and excitation in thalamocortical microcircuits. *Prog. Brain Res.* **213**, 223–252 (2014).
48. Paz, J. T. et al. A new mode of corticothalamic transmission revealed in the Gria4(-/-) model of absence epilepsy. *Nat. Neurosci.* **14**, 1167–1173 (2011).
49. Mangan, K. P. et al. Tonic inhibition is abolished in GAB_{AA} receptor γ2R43Q knock-in mice with absence epilepsy and febrile seizures. Preprint at bioRxiv https://www.biorxiv.org/content/early/2017/06/26/155556 (2017).
50. Guo, J. N. et al. Impaired consciousness in patients with absence seizures investigated by functional MRI, EEG, and behavioural measures: a cross-sectional study. *Lancet Neurol.* **15**, 1336–1345 (2016).

Acknowledgements

We wish to thank T. Gould for technical assistance and V. N. Uebele (Merck Inc., USA) for the generous gift of TTA-P2. This work was supported by the MRC (grant G0900671 to V.C.), the Wellcome Trust (grant 91882 to V.C.), the Hungarian Scientific Research Fund (grant NN125601 to M.L.L.), the Hungarian Brain Research Program (grant KTIA_NAP_13-2-2014-0014 to M.L.L.), the CNRS (grant LIA 528 to N.L., R.C.L. and V.C.), the European Union (grant COST Action CM1103 to G.D.G.) and the Malta Council of Science and Technology (MCST, grant R&I-2013-14 "EPILEFREE" to G.D.G. and V.C.). M.V. and Z.A. were supported by Wellcome Trust 4-year PhD studentships (grants 93763 and 204014, respectively) and F.D. by a Marie Curie ITN PhD studentship (grant H2020-MSCA-ITN-2016 -722053).

Author contributions

C.M.C., F. David, M.L.L., R.C.L., G.D.G., N.L. and V.C. designed research and experiments; C.M.C., F. David, M.V., M.L.L., G.O., F. Delicata, Z.A., G.R., G.D.G. and N.L. performed experiments and analyzed data; C.M.C., F. David and V.C. wrote the manuscript with critical review by other authors.

Competing interests

The authors declare no competing financial interests.

Additional information

Supplementary information is available for this paper at https://doi.org/10.1038/s41593-018-0130-4.

Reprints and permissions information is available at www.nature.com/reprints.

Correspondence and requests for materials should be addressed to C.M. or V.C.

Publisher's note: Springer Nature remains neutral with regard to jurisdictional claims in published maps and institutional affiliations.

Methods

Animals. Experiments were approved under the UK Animals (Scientific Procedures) Act 1986 by Cardiff University Animal Welfare and Ethics Committee and were conducted in accordance with current recommendations for experimental work in epilepsy[51].

No statistical methods were used to predetermine sample sizes, but our sample sizes are similar to those reported in previous publications[25,34]. In the case of bilateral microdialysis experiments, animals were randomly assigned to receive drug or control first. Experimenters were blind to the group of animals when detecting time spent in seizure. Animals were excluded from microdialysis experiments only in the case of visible distress, and neurons were excluded from ensemble recording experiments if the reconstructed electrode position lay outside the VB or NRT.

Surgery and implantation. Male GAERS and Wistar rats (both 4–7 month old), with access to food and water ad libitum, were maintained on a 12:12 h light:dark cycle (light on at 8:00 a.m.). Surgery anesthesia was maintained with isoflurane and body temperature with a homoeothermic heat blanket. EEG gold-plated screws (Svenska Dentorama, UK) were implanted in fronto-parietal sites.

For ensemble unit recordings, four-shank, linear, 32-site silicon probes (Buzsaki32L, NeuroNexus, Michigan, USA) were immersed in detergent at 60 °C for 2–4 h before being rinsed with deionized water and immersed in Vybrant DiI dye (Invitrogen) solution before insertion (Supplementary Fig. 1c). Each silicon probe was lowered into the VB (AP: −3.35 mm, ML: 2.9 mm)[52], such that its lower end rested 4 mm ventral to the brain surface; i.e., at the top of the VB. A microdrive was then secured with grip cement that was also used to create a mini-Faraday cage and protective structure of copper mesh[53]. When an additional silicon probe was implanted in S1pO cortex, its coordinates were AP: −0.0 mm, ML: 5.5 mm and its tip was initially positioned in cortical layer 2/3.

For experiments with bilateral microdialysis, two guide cannulae for CMA 12 microdialysis probes (Linton Instruments, UK) were lowered into the center of the VB (Fig. 7b), such that their tips rested at AP: −3.35 mm, ML: 2.8 mm, DV: −4.4 mm. To target the NRT, probes were positioned adjacent to but not within the NRT so as to avoid excessive damage to this narrow nucleus (AP: −3.2 mm, ML: 3.5 mm, DV: −4.2 mm). The coordinates for the probes positioned more medially than the center of the VB (Fig. 7b) were AP: −3.35 mm, ML: 2.1 mm, DV: −4.4 mm, and those targeting S1pO cortex were AP: −3.2 mm, ML: 5.5 mm, DV: −0.5 mm.

Simultaneous unilateral implantation of a silicon probe and a microdialysis cannula was similar to the one described above, with the microdialysis cannula being lowered into the brain at a 16° angle with respect to the vertical axis in the rostro-caudal plane such that its tip rested close to the silicon probe (AP −3.5 mm, ML 2.8 mm, DV −6 mm)[20].

All electrical and microdialysis components were affixed to the skull with methylacrylic cement, and the final cap structure incorporated all electrode wires and microdialysis guide cannulae. Rats were allowed to recover for ≥5 d.

Behavioral experiments. For all behavioral experiments, each animal was placed individually in a purpose-built Plexiglas box housed within a Faraday cage. Animals were continuously monitored throughout a procedure by an experimenter and by video recordings (using Spike2 video software, CED, Cambridge, UK) to precisely time-match EEG and neuronal ensemble recordings with behavior (see below). A counterweighted swivel arm positioned above the recording box allowed free movement of the animal while the animal was connected to electrical and microdialysis equipment.

Neuronal ensemble recordings. The head-mounted Plexon HST/32V-G20 VLSI-based preamplifier was connected to a Plexon data acquisition system (sampling rate: 20 kHz). Online filtering was used to visualize the raw signal as either LFP (low-pass filter at 300 Hz) or as spiking unit activity (high-pass filter at 500 Hz). Upon connection to the recording apparatus, the presence or absence (on any channel) of neurons suitable for recording was assessed based on the shape and amplitude of any visible spikes. If no such neurons were present after 30 min of observation, the silicon probe was lowered deeper into the brain by turning the microdrive while recording the number and degree of turns of the microdrive screw to allow post hoc reconstruction of the recording site (see below). A similar procedure was used for simultaneous recordings of thalamic and cortical neurons.

For GAERS rats, each recording session lasted no more than 3 h, depending on the quality and stability of the recorded neurons and the behavior of the animal during the session. In the GHB model (100 mg/kg i.p. of γ-butyrolactone, a GHB prodrug), recordings were limited by the time course of the drug (about 1 h). GAERS sessions included multiple bouts of non-REM sleep, which were used to characterize the properties of the T-channel-mediated high-frequency bursts of each recorded thalamic neuron for subsequent comparison with the high-frequency bursts recorded from the same neuron during multiple ASs (see below).

Bilateral reverse microdialysis. Dummy probes in the guide cannulae were replaced with CMA 12 microdialysis probes (Linton Instruments, UK) 18 h before the start of a recording session. For GAERS rats, each experiment involved 1 h habituation of the animal to the recording environment after the inlet tubes of the microdialysis probes had been connected (via FEP tubing, 0.18 µL/cm internal volume, Linton Instruments, UK) to a 1 mL syringe placed in a four-channel microdialysis pump (CMA 400, Linton Instruments, UK). The second hour consisted of EEG recording during reverse microdialysis of artificial cerebrospinal fluid (aCSF) at a rate of 1 µL/min. At the end of the second hour, either reverse microdialysis of aCSF was continued or a solution containing TTA-P2 (300 µM or 1 mM) or CGP-55845 (500 µM) was administered via different syringes for another 80 min.

A minimum delay of 6 d occurred between subsequent experiments to allow wash-out of the drug. Each animal was recorded twice only, once with aCSF and once with TTA-P2 administration, and was randomly allocated to receive first aCSF or TTA-P2. The effect of TTA-P2 was quantified during the 40–80 min period ('treatment hour') (Fig. 7e) from the start of its microdialysis, since our previous experiments under similar conditions had shown that 20 min are necessary to achieve a steady blockade of TC neuron burst firing throughout the required extent of the VB (see ref. [37] for more information). Effects of microdialysis-applied TTA-P2 on ASs are reported as percentage of values during the aCSF treatment (Fig. 7e,f).

Simultaneous neuronal ensemble recordings and unilateral reverse microdialysis. Silicon electrodes were employed as described earlier for neuronal ensemble recordings. Microdialysis probe cannulae were inserted as described above, so that the membrane of the microdialysis probe would extend beneath the VB thalamus, allowing the silicon electrode to be moved gradually toward the membrane by microdrive adjustment[20]. Upon identification of suitable and stable neurons, a recording control period was carried out before 300 µM TTA-P2 was administered. Neuronal firing dynamics were investigated as described below for the periods before and after full blockade of bursts by TTA-P2 had been detected.

Data analysis. *AS detection and SWD analysis.* The EEG was recorded using an SBA4-v6 BioAmp amplifier (SuperTech Inc., Hungary), digitized at 1 kHz by a Cambridge Electronic Design (CED) Micro3 D.130 and analyzed with CED Spike2 v7.3 and Matlab (R2011b, The MathWorks Inc., USA). SWDs were identified using the SeizureDetect script (Spike2, CED, Cambridge, UK). First, baseline EEG (desynchronized, active or resting wakefulness) was identified manually and voltage amplitude thresholds set at 5–7 s.d. above or below the mean. Second, the following parameters for initial event detection were applied to all points that crossed this threshold (crossings): maximum time between initial two crossings of 0.2 s, maximum time between any two crossings within an event of 0.35 s, minimum of five crossings per event, minimum time of 0.5 s between any two events for them to count as separate (otherwise overriding the 0.35-s limit and merging events) and a minimum event duration of 1 s. The final component of the SeizureDetect script gated detected events by dominant frequency band (calculated by time intervals between crossings rather than by spectrographic analysis). Events with >75% of intervals within the 5–12 Hz range were classified as SWDs. Designated SWDs were then visually inspected to ensure the above parameters and the signal-to-noise ratio were appropriate for effective identification and isolation. All EEG sections identified as SWDs were then crossed-checked with the corresponding video recordings: those that showed the concurrent presence of behavioral arrest were then classified as ASs, while the very few that did not were excluded from further analysis.

Behavioral state classification. EEG recordings were divided into one of three behavioral states: non-REM sleep, wakefulness and ASs. Isolation of ASs (i.e., concomitant presence of behavioral arrest and SWDs in the EEG) was carried out as detailed above. Detection of non-REM sleep periods, from the sections of the EEG and video recordings that did not contain ASs, was achieved by plotting cumulative power over the 0.5 to 4 Hz frequency range of the EEG signal and setting a threshold at 2.5 s.d. above the baseline value during a visually identified period of wakefulness, along with post hoc analysis of the video recordings. The remaining time (i.e., neither ASs or non-REM sleep) was classified as wakefulness upon confirmation of a desynchronized (low amplitude, high frequency) EEG. Note that ASs only developed during wakefulness, and thus the pre-ictal periods used for the analysis of interictal-to-ictal transitions only included wakefulness. Periods of non-REM sleep were extremely rare in GHB-injected Wistar rats due to the relatively short duration (about 1 h) of the recording period.

Action potential sorting. Extraction of action potentials was performed with different subroutines[20,24]. The signal was high-pass filtered and thresholded to extract action potential shapes (Fig. 1b and Supplementary Fig. 1a), using the first three principal components of each action potential on each channel (eight channels per group for the Buzsaki32L probe) as features. The first stage of clustering used the unsupervised KlustaKwik program[54] to group action potentials with similar features into clusters based on a classification expectation maximization (CEM) algorithm[55–59] (Fig. 1a). The second stage involved supervised refinement of appropriate clusters and elimination of unsuitable clusters. Action potential waveforms were constant and distinct during non-REM sleep and wakefulness but some would at times be insufficiently large, relative to the high-frequency multi-unit noise observed at each SWC cycle, to sort during ASs. In this case the entire cluster was eliminated.

Neuron and firing pattern classifications. For thalamic neurons, isolated action potentials recorded from locations outside the VB or NRT region were excluded from further analysis. The remaining action potentials were classified as attributable to TC neurons or fibers belonging to NRT neurons[25] on the basis of (i) the properties of their T-channel dependent high-frequency bursts during non-REM sleep (Supplementary Fig. 1e), (ii) the action potential half-width (Fig. 1d) and (iii) the ratio of the first to the shortest interspike interval (ISI) (Fig. 1d). A high-frequency burst was defined as three or more spikes with an ISI of ≤7 ms that were preceded by a silent interval of ≥100 ms. NRT neurons were classified as those with an acceleration index (ratio of first to shortest ISIs in a burst) > 1.4 while TC neurons have an index <1.3 (refs [60,61]) (Fig. 1d). Moreover, NRT neurons tended to exhibit a smaller spike half-width than TC neurons (Fig. 1d). These properties are in agreement with the previously reported 'accelerando–decelerando' pattern of NRT bursts[60,61] (Fig. 1c and Supplementary Fig. 1d) and the sharper waveform of the action potentials of inhibitory compared to excitatory neurons[25,62] (Fig. 1d, inset).

Total firing reported in the text and figures for both types of thalamic neurons includes all sorted spikes while tonic firing includes all spikes separated by two ISIs > 7 ms in order to discard spike potentially belonging to bursts. Action potential doublets that did not fall into the tonic firing classification were post hoc included in all burst firing calculations because of the marked similarity of their temporal dynamics before, during and after ASs with bursts of ≥3 action potentials (Supplementary Fig. 1e). A proportion of spikes could not be conclusively classified as being either burst or tonic firing, and amounted to the following percentages: GAERS TC neurons: 10.0 ± 8.9%; wake-active NRT neurons: 4.1 ± 0.8%; wake-quiescent NRT neurons: 2.4 ± 1.5%; GHB TC neurons: 2.48 ± 2.27%; wake-active NRT neurons: 9.7 ± 3.5%; wake-quiescent NRT neurons: 3.7 ± 0.4%. These spikes, however, were all included in the total firing.

Burst, tonic and total firing rates in each of the three behavioral conditions, as well as during transitions between conditions, were calculated across entire recording sessions (Supplementary Table 1). Transitions from wakefulness to seizure and vice versa were investigated by plotting mean activity rates (±s.e.m.) 5 s before and after seizure start and end times, respectively. Only seizures of duration ≥5 s (for GAERS) or ≥2 s (for GHB) with preceding or following (as appropriate) wake periods of at least the same length were selected.

For cortical neurons, isolated neurons were classified as putative excitatory cells and distinguished from putative inhibitory cells on the basis of their trough-to-peak times and spike half-widths[62] (Supplementary Fig. 9). Functional somatotopic alignment of the thalamic and cortical regions was verified by sending brief air puffs to the perioral zone of the GAERS rats. Most neurons in both brain regions responded within 10 ms to this sensory stimulation.

Neuron–neuron and neuron–EEG relationships were investigated during each behavioral state, with neuron–SWC relationships also studied during ASs. Auto- and cross-correlograms (XCors) were calculated using the xcorr function of Matlab in 1-ms bins. SWC spike-triggered EEG averages were calculated by taking mean values of ictal total, tonic and burst rates (burst time taken as time of first spike in a burst) across entire recording sessions and then averaging across all neurons of the same type (TC, WA NRT, WQ NRT). SWC spike-triggered firing averages used the SWC spike as reference. This involved finding all local amplitude maxima more than 3 s.d. above the mean EEG amplitude and then selecting the largest of these maxima within each SWC. Spike and burst rates were averaged in 1-ms bins around these peaks. Other measures that quantified activity relative to the SWC required definition of SWC epochs. These were extrapolated from spike peak detections by selecting periods between adjacent peaks with intervals less than 300 ms. These epochs were used to calculate per-SWC total firing, tonic firing and bursts across entire recording sessions.

Coherence. Total firing, burst firing and tonic firing distribution were selected between −70 and 70 ms around the SWC spike time and normalized to get the density distribution binned per ms. Vectors were then circularized by linearly converting the −70 to +70 ms interval into an angle from $-\pi$ to π. The module of the average vector computed over all density values at each angle bin was then estimated in the complex domain to give the coherence. This measure is comparable to a spike–field coherence[63].

SWC-spike amplitude. The amplitude of the SWC spikes was measured from the EEG recordings. Neuronal spikes used for cross-correlations based on SWC-spike amplitudes were extracted from periods around those SWCs of the smallest (first) and largest (fourth) quartiles (Fig. 6e,f and Supplementary Fig. 10b,c). Analyses of the XCors were done for pairs of neurons that had an amplitude 20 ms around the time lag = 0 ms of at least 8 times the basal chance level found beyond 20 ms away from lag = 0. This ensured that thalamic and cortical neurons fired in a correlated manner for the directional analysis. Out of 58 TC–cortical pairs, 24 satisfied this criterion. Then peak ratios were measured as ratios between (i) the maximum amplitudes corresponding to time lags between −10 ms and 0 ms in the XCors for the thalamo-cortical direction measurement and to time lags between 0 and 10 ms in the XCors for the cortico-thalamic direction measurement for either the first or fourth quartile, and (ii) the same measurement for all SWCs no matter their amplitude. Those values were then normalized per SWC. The resulting peak ratios indicate changes in the strengths of thalamo-cortical (TC) (Fig. 6d) and cortico-thalamic (CX) (Fig. 6e) interactions with respect to changes in the amplitude of the SWC spike. Lastly, a ratio was computed between CX and TC unidirectional peak ratio (Fig. 6f).

Histological processing. For animals used in the microdialysis experiments, 1 µL of thionine dye was administered via both inlet and outlet channels of the microdialysis probes with stripped membranes using a 10-µL Hamilton syringe to highlight the probes' tracks. At the end of all experiments, animals received lethal doses of Euthatal before being transcardially perfused with phosphate-buffered saline (PBS, 0.9% NaCl) followed by paraformaldehyde (PFA, buffered in 0.9% NaCl PBS). Microdialysis and/or silicon probes were then carefully withdrawn from the brain, which was then immersed in 4% PFA for 4 h. Brains were refrigerated in 0.9% NaCl PBS until required. Brain sections around the region of interest were cut at a thickness of 100 µm on a Leica VT 1000 S vibratome while immersed in chilled 0.9% NaCl PBS. For microdialysis experiments, slices were photographed using a Nikon D90 camera (Nikon Imaging, UK) and then inspected for the actual site of recording. For neuronal ensemble recording experiments, slices were photographed under an Olympus BX61 microscope at 4× magnification in brightfield and with a TRITC filter. Images were merged using Adobe Photoshop (Supplementary Fig. 1c), and the final position of the electrode tip was marked. The position of the recording site during each session was then calculated from the noted microdrive movements.

Drugs. The aCSF for the microdialysis experiments was purchased from Tocris Biosciences (Bristol, UK). 3,5-Dichloro-*N*-[1-(2,2-dimethyl-tetrahydro-pyran-4-ylmethyl)-4-fluoro-piperidin-4-yl-methyl]-benzamide (TTA-P2) was a kind gift from Merck Inc. (USA). TTA-P2 was dissolved in DMSO (2% of final solution) before addition to aCSF. An identical concentration of DMSO was added to the aCSF solutions. (2*S*)-3-[[(1*S*)-1-(3,4-dichlorophenyl)ethyl]amino-2-hydroxypropyl](phenylmethyl)phosphinic acid hydrochloride (CGP-55845) was purchased from Tocris (UK). The pH of all dialysis solutions was 7.

Simulations. Using Neuron software[64], a previously developed[39] single-compartment conductance model of a TC neuron was connected to two NRT neuron models[65] and to two cortical pyramidal neuron (PY) models[66], which were also connected to the TC neuron and the two NRT neurons (Fig. 8a; see Supplementary Table 3 for network description and synapse properties). T-type Ca^{2+} channels had a conductance of 40 nS and a reversal potential of 120 mV in TC neurons. The two NRT neurons received different constant current injections to set their membrane potential in a different range, thus favoring (NRT2) or not (NRT1) the emergence of T-channel bursts. Single AMPA synapses from TC to NRT neurons and single $GABA_A$ synapses from NRT to the TC neuron were similar to those described in ref. [65]. AMPA synapses from TC to CX, from CX to TC, and from CX to NRT were modeled as single exponential conductances (ExpSyn object in Neuron with a decay time constant of 2 ms), with a transmission delay of 2 ms to represent inter-area communications. Their synaptic weights were either 0, when connections were inactive, or as reported in Supplementary Table 3. All neurons also received synaptic-conductance fluctuating noisy inputs[65,67,68]. The mean conductance of the synaptic noise was set as 20% of g_{Leak} for excitatory noise and 80% of g_{Leak} for inhibitory noise for all neurons[39]. The s.d. of the synaptic noise was set to 100%, 60%, and 150% of the mean conductance for TC, NRT and PY neurons, respectively, in order to induce fluctuations of spike timing that reflect those observed in the experimental data. The synaptic weight of the cortico-thalamic EPSPs was adjusted to induce a spiking probability similar to that of our experimental data (Supplementary Table 3). All neurons had T-type Ca^{2+} channels and thus were able to generate rebound bursts after a hyperpolarizing pulse.

In addition to those basal conditions of the cortico-thalamic network described above, which reflect the interictal neuronal state, the two PY model neurons received identical inputs consisting of trains of five AMPA EPSPs (modeled as in ref. [51]). No other external input was delivered to either the TC or the NRT neurons. The inter-EPSP interval within a train was randomly drawn from a Poisson distribution with a mean of 3 ms. The inter-train interval was randomly drawn from a Poisson distribution with a mean of 140 ms, which produced an average frequency of 7 Hz, similar to the SWD frequency in GAERS rats. Twenty-second-long simulations were repeated 40 times with different noise seeds. Simulated firing activity was analyzed as the experimental data. Time zero for the simulated firing distribution plots was taken as the third EPSPs of a train; selecting either earlier or later EPSPs in the train had no major effects on the simulation results.

Statistical analysis. A paired Wilcoxon signed-rank test was used for the effect of TTA-P2 on TC neuron firing and ASs. Circular statistics (Kuiper test and concentration factors) was used to compare phase distributions across the SWC epoch (Fig. 7d and Supplementary Fig. 12a,c). A Kolmogorov–Smirnov test was used for spike time distribution around the SWC spike (Fig. 4). Normality and equal variances were not assumed by the tests employed.

Permutations were used for non-parametric tests applied to compare experimental XCors to XCors expected if spikes were to occur at times drawn randomly from their distribution around the SWC spike time (Figs. 5, 6 and 8 and

Supplementary Figs. 8 and 10a). The same number of spike time pairs as in the experimental XCors is drawn from the respective TC, NRT and cortical neuron density distributions around the SWC spike time. Computing their XCors allowed us to generate a surrogate XCor wherein spikes are shuffled independently from each other but respecting the probability distribution of finding them at particular times around the SWC spike time. Repeating the process 1,000 times allowed us to estimate the 5% and 95% limits (confidence interval) for the surrogate XCor that could be directly compared to experimental XCors. This method is more stringent than simple spike-time shuffling around their measured times[69], since it takes into account specific spike times associated to an external source of synchronization that can generate peaks and troughs without any direct relationships between neurons.

Reporting Summary. Further information on experimental design is available in the Nature Research Reporting Summary linked to this article.

Data and code availability. All data included in this publication or MatLab code used for the analysis will be made available on reasonable request by contacting one of the corresponding authors.

References

51. Lidster, K. et al. Opportunities for improving animal welfare in rodent models of epilepsy and seizures. *J. Neurosci. Methods* **260**, 2–25 (2016).
52. Paxinos, G. & Watson, C. *The Rat Brain in Stereotaxic Coordinates* 6th edn. (Academic, New York, 2007).
53. Vandecasteele, M. et al. Large-scale recording of neurons by movable silicon probes in behaving rodents. *J. Vis. Exp.* **2012**, e3568 (2012).
54. Harris, K. D., Henze, D. A., Csicsvari, J., Hirase, H. & Buzsáki, G. Accuracy of tetrode spike separation as determined by simultaneous intracellular and extracellular measurements. *J. Neurophysiol.* **84**, 401–414 (2000).
55. Celeux, G. & Govaert, G. A classification EM algorithm for clustering and two stochastic versions. *Comput. Stat. Data Anal.* **14**, 315–332 (1992).
56. Henze, D. A. et al. Intracellular features predicted by extracellular recordings in the hippocampus in vivo. *J. Neurophysiol.* **84**, 390–400 (2000).
57. Pedreira, C., Martinez, J., Ison, M. J. & Quian Quiroga, R. How many neurons can we see with current spike sorting algorithms? *J. Neurosci. Methods* **211**, 58–65 (2012).
58. Pouzat, C., Delescluse, M., Viot, P. & Diebolt, J. Improved spike-sorting by modeling firing statistics and burst-dependent spike amplitude attenuation: a Markov chain Monte Carlo approach. *J. Neurophysiol.* **91**, 2910–2928 (2004).
59. Schmitzer-Torbert, N., Jackson, J., Henze, D., Harris, K. & Redish, A. D. Quantitative measures of cluster quality for use in extracellular recordings. *Neuroscience* **131**, 1–11 (2005).
60. Domich, L., Oakson, G. & Steriade, M. Thalamic burst patterns in the naturally sleeping cat: a comparison between cortically projecting and reticularis neurones. *J. Physiol. (Lond.)* **379**, 429–449 (1986).
61. Steriade, M., Domich, L. & Oakson, G. Reticularis thalami neurons revisited: activity changes during shifts in states of vigilance. *J. Neurosci.* **6**, 68–81 (1986).
62. Barthó, P. et al. Characterization of neocortical principal cells and interneurons by network interactions and extracellular features. *J. Neurophysiol.* **92**, 600–608 (2004).
63. Vinck, M., Battaglia, F. P., Womelsdorf, T. & Pennartz, C. Improved measures of phase-coupling between spikes and the local field potential. *J. Comput. Neurosci.* **33**, 53–75 (2012).
64. Hines, M. L. & Carnevale, N. T. NEURON: a tool for neuroscientists. *Neuroscientist* **7**, 123–135 (2001).
65. Destexhe, A., Bal, T., McCormick, D. A. & Sejnowski, T. J. Ionic mechanisms underlying synchronized oscillations and propagating waves in a model of ferret thalamic slices. *J. Neurophysiol.* **76**, 2049–2070 (1996).
66. Destexhe, A., Contreras, D. & Steriade, M. LTS cells in cerebral cortex and their role in generating spike-and-wave oscillations. *Neurocomputing* **38**, 555–563 (2001).
67. Wolfart, J., Debay, D., Le Masson, G., Destexhe, A. & Bal, T. Synaptic background activity controls spike transfer from thalamus to cortex. *Nat. Neurosci.* **8**, 1760–1767 (2005).
68. Destexhe, A., Mainen, Z. F. & Sejnowski, T. J. Synthesis of models for excitable membranes, synaptic transmission and neuromodulation using a common kinetic formalism. *J. Comput. Neurosci.* **1**, 195–230 (1994).
69. Fujisawa, S., Amarasingham, A., Harrison, M. T. & Buzsáki, G. Behavior-dependent short-term assembly dynamics in the medial prefrontal cortex. *Nat. Neurosci.* **11**, 823–833 (2008).

nature research

Corresponding author(s): Vincenzo Crunelli

Reporting Summary

Nature Research wishes to improve the reproducibility of the work that we publish. This form provides structure for consistency and transparency in reporting. For further information on Nature Research policies, see Authors & Referees and the Editorial Policy Checklist.

Statistical parameters

When statistical analyses are reported, confirm that the following items are present in the relevant location (e.g. figure legend, table legend, main text, or Methods section).

n/a	Confirmed	
☐	☒	The exact sample size (*n*) for each experimental group/condition, given as a discrete number and unit of measurement
☐	☒	An indication of whether measurements were taken from distinct samples or whether the same sample was measured repeatedly
☐	☒	The statistical test(s) used AND whether they are one- or two-sided *Only common tests should be described solely by name; describe more complex techniques in the Methods section.*
☐	☒	A description of all covariates tested
☐	☒	A description of any assumptions or corrections, such as tests of normality and adjustment for multiple comparisons
☐	☒	A full description of the statistics including central tendency (e.g. means) or other basic estimates (e.g. regression coefficient) AND variation (e.g. standard deviation) or associated estimates of uncertainty (e.g. confidence intervals)
☐	☒	For null hypothesis testing, the test statistic (e.g. *F*, *t*, *r*) with confidence intervals, effect sizes, degrees of freedom and *P* value noted *Give P values as exact values whenever suitable.*
☐	☒	For Bayesian analysis, information on the choice of priors and Markov chain Monte Carlo settings
☐	☒	For hierarchical and complex designs, identification of the appropriate level for tests and full reporting of outcomes
☐	☒	Estimates of effect sizes (e.g. Cohen's *d*, Pearson's *r*), indicating how they were calculated
☐	☒	Clearly defined error bars *State explicitly what error bars represent (e.g. SD, SE, CI)*

Our web collection on statistics for biologists may be useful.

Software and code

Policy information about availability of computer code

Data collection	Spike2 v7 (CED) and Omniplex v1.9 (Plexon) were used to collect the data in this study.
Data analysis	Spike2 v7 (CED), MatLab R2015b (Mathworks), KlustaKwik v1.5 (Ken Harris), and Neurosuite v2.0 (Neuroscope, Klusters, and NDManager by Lynn Hazan and Michael Zugaro) were used to process and analyze data.

For manuscripts utilizing custom algorithms or software that are central to the research but not yet described in published literature, software must be made available to editors/reviewers upon request. We strongly encourage code deposition in a community repository (e.g. GitHub). See the Nature Research guidelines for submitting code & software for further information.

Data

Policy information about availability of data

All manuscripts must include a data availability statement. This statement should provide the following information, where applicable:

- Accession codes, unique identifiers, or web links for publicly available datasets
- A list of figures that have associated raw data
- A description of any restrictions on data availability

All data (and code used to analyze data) are readily available from a corresponding author upon request.

Field-specific reporting

Please select the best fit for your research. If you are not sure, read the appropriate sections before making your selection.

☒ Life sciences ☐ Behavioural & social sciences

For a reference copy of the document with all sections, see nature.com/authors/policies/ReportingSummary-flat.pdf

Life sciences

Study design

All studies must disclose on these points even when the disclosure is negative.

Sample size	No statistical methods were used to pre-determine sample sizes but our sample sizes are similar to those reported in previous publications including Paz et al (Nat Neuro, 2011) and Cope et al (Nat Med, 2009)
Data exclusions	Animals were excluded from microdialysis experiments only if there was excessive damage caused by the microdialysis probe's insertion (including causing bleeding or widespread tissue damage as assessed histologically). No animals were excluded from unit recording experiments. Neurons were excluded from unit recording experiments if histological reconstruction showed them to be outside the target regions (cortex, VB thalamus, NRT) or if their recording did not allow their classification due to short duration or aberrant behavior.
Replication	Replication of the unit recording findings relies upon the collection of neuronal data from independent animals at different times. The microdialysis experiments were not replicated, as is standard in the field.
Randomization	Animals in microdialysis experiments were randomly assigned to receive control or drug infusion first. All animals received both, so no group assignment was necessary.
Blinding	Investigators were blind to the drug administered during seizure detection for microdialysis experiments. Blinding during drug administration was not possible due to the differing appearances of the aCSF and dissolved TTA-P2.

Materials & experimental systems

Policy information about availability of materials

n/a	Involved in the study
☐	☒ Unique materials
☒	☐ Antibodies
☒	☐ Eukaryotic cell lines
☐	☒ Research animals
☒	☐ Human research participants

Unique materials

Obtaining unique materials	TTA-P2 was, at the time of the experiments, a gift from Merck Inc. It is now commercially available.

Research animals

Policy information about studies involving animals; ARRIVE guidelines recommended for reporting animal research

Animals/animal-derived materials	GAERS and Wistar rats used were all between 4 and 7 month old males.

Method-specific reporting

n/a	Involved in the study
☒	☐ ChIP-seq
☒	☐ Flow cytometry
☒	☐ Magnetic resonance imaging